



저작자표시-비영리-변경금지 2.0 대한민국

이용자는 아래의 조건을 따르는 경우에 한하여 자유롭게

- 이 저작물을 복제, 배포, 전송, 전시, 공연 및 방송할 수 있습니다.

다음과 같은 조건을 따라야 합니다:



저작자표시. 귀하는 원저작자를 표시하여야 합니다.



비영리. 귀하는 이 저작물을 영리 목적으로 이용할 수 없습니다.



변경금지. 귀하는 이 저작물을 개작, 변형 또는 가공할 수 없습니다.

- 귀하는, 이 저작물의 재이용이나 배포의 경우, 이 저작물에 적용된 이용허락조건을 명확하게 나타내어야 합니다.
- 저작권자로부터 별도의 허가를 받으면 이러한 조건들은 적용되지 않습니다.

저작권법에 따른 이용자의 권리는 위의 내용에 의하여 영향을 받지 않습니다.

이것은 [이용허락규약\(Legal Code\)](#)을 이해하기 쉽게 요약한 것입니다.

[Disclaimer](#)

공학석사 학위논문

**Development of Sectional Analysis
Platform for Reinforced and
Prestressed Concrete Elements**

철근콘크리트와 프리스트레스트 콘크리트

단면해석 플랫폼 구축 연구

2017 년 8 월

서울대학교 대학원

건축학과

이 주 홍

Abstract

Development of Sectional Analysis Platform for Reinforced and Prestressed Concrete Elements

Lee, Joo Hong

Department of Architecture and Architectural Engineering
College of Engineering
Seoul National University

Prestressing has become one of the most important reinforcement methods for concrete elements. However the research for analyzing the sectional behavior of a prestressed concrete element has not been thorough yet. Three dimensional finite element method could be one of the means to understand the behavior, but computational cost is too high. Therefore, simple lumped plasticity modeling is necessary for analyzing a multi-story building system with prestressed elements and performing its displacement-based seismic design. In this study, a computer program with new analytic models is developed focusing on the generation of moment-curvature relation and axial force-moment (P-M) interaction that may be used for the performance-based design. A new analytic model regarding the relation between tendon stress increase and element load/moment is established from the collated previous experimental results. The program is well-designed for users to calculate the moment-curvature relations and P-M interactions of various reinforced and

prestressed concrete sections, including unbonded prestressed element sections. The generated data from the program when it comes to normal reinforced concrete elements and bonded prestressed concrete elements are reasonable and accurate, comparing with the previously verified program and other projects. On the other hand, the sectional analysis of unbonded prestressed elements is unprecedented. Through the case study with various analysis options, it is shown that linear and exponential tendon stress increase models can be recommended. This study focuses on the convergence research of computer programming and structural engineering through development of the sectional analysis program supporting most cases of structural elements.

Keywords: sectional analysis, reinforced concrete, bonded prestressed concrete, unbonded prestressed concrete, moment-curvature relation, P-M interaction

Student Number: 2015-22847

Contents

Abstract	i
Contents	iii
List of Tables	vi
List of Figures	vi
List of Symbols	x
Chapter 1. Introduction	1
Chapter 2. Review of Previous Studies	3
2.1 Design Code.....	3
2.2 Previous Studies.....	5
2.2.1 Concrete material models	5
2.2.1.1 Hognestad (1951) confined concrete model	6
2.2.1.2 Modified Kent and Park concrete model	8
2.2.1.3 Popovics (1973) unconfined concrete model.....	11
2.2.1.4 Saatcioglu and Razvi (1992) confined concrete model	13
2.2.1.5 Yang et al. (2014) unconfined concrete model	17
2.2.2 Steel material models	19
2.2.2.1 Bilinear steel model	20
2.2.2.2 Ramberg-Osgood (1943) steel model	21
2.2.2.3 Menegotto-Pinto steel model	23
2.2.3 Prestressing steel or tendon material model	25

2.2.3.1 PCI tendon model	26
2.2.3.2 Mattock tendon model	28
2.3 Summary	30

Chapter 3. Experimental Data Assessment for Unbonded Post-Tensioned Members 31

3.1 Experimental Data	31
3.1.1 Foutch et al. (1990)	32
3.1.2 Lee et al. (2010).....	33
3.1.3 Burns et al. (1978).....	34
3.1.4 Zhou and Zheng (2014).....	35
3.1.5 Tao and Du (1985).....	36
3.1.6 Lim et al. (1999).....	37
3.2 Empirical Model Development.....	38
3.3 Summary	41

Chapter 4. Program Development..... 43

4.1 Purpose and Outline.....	43
4.2 Program Structures	44
4.3 Material and Section Configuration.....	47
4.4 Performing Analysis	50
4.4.1 General analysis process	50
4.4.2 Prestressed elements with unbonded tendons.....	53
4.5 Example of Results of Analysis	57
4.6 Summary	59

Chapter 5. Analysis Results and Verification..... 61

5.1 Verification Using Cases with Various Conditions	64
5.1.1 Unconfined reinforced concrete section.....	64
5.1.2 Confined reinforced concrete section.....	68

5.1.3 Bonded prestressed concrete section.....	71
5.2 Discussion.....	74
5.2.1 Case study 1	76
5.2.2 Case study 2	80
5.2.3 Summary	84
Chapter 6. Conclusion.....	85
References	86
Appendix A: Program Screenshots and Detailed Description	89
Appendix B: Simple User Manual for Program	101
국 문 초 록.....	106

List of Tables

Table 4-1 Major class names and roles	44
Table 4-2 Details of analysis options.	52
Table A-1 Menu description.....	90

List of Figures

Figure 1-1 Longitudinal cross section of prestressed concrete.....	1
Figure 1-2 Plastic hinge of structural element.....	2
Figure 2-1 Strain compatibility description.....	3
Figure 2-2 Compression zone approximation.....	4
Figure 2-3 Normal concrete (28 MPa) stress-strain diagram by Hognestad confined concrete model.....	7
Figure 2-4 Normal concrete (28 MPa) stress-strain diagram by modified Kent and Park concrete model	10
Figure 2-5 Normal concrete (28 MPa) stress-strain diagram by Popovics unconfined concrete model.....	12
Figure 2-6 Normal concrete (28 MPa) stress-strain diagram by Saatcioglu and Razvi model	16
Figure 2-7 Normal concrete (28 MPa) stress-strain diagram by Yang et al. unconfined concrete model.....	18
Figure 2-8 400 MPa steel rebar stress-strain diagram by bilinear model	20
Figure 2-9 400 MPa steel rebar stress-strain diagram by Ramberg-Osgood model.....	22
Figure 2-10 400 MPa steel rebar stress-strain diagram by Menegotto-Pinto model.....	24
Figure 2-11 1750 MPa tendon stress-strain diagram by PCI tendon model	27
Figure 2-12 1860 MPa tendon stress-strain diagram by Mattock model	

.....	29
Figure 3-1 Experimental results from Foutch et al. (1990)	32
Figure 3-2 Experimental results from Lee et al. (2010)	33
Figure 3-3 Experimental results from Burns et al. (1978).....	34
Figure 3-4 Experimental results from Zhou and Zheng (2014).....	35
Figure 3-5 Experimental results from Tao and Du (1985).....	36
Figure 3-6 Experimental results from Lim et al. (1999).....	37
Figure 3-7 Interaction diagram of normalized tendon stress increase and normalized load or moment	38
Figure 3-8 Normalized original experimental data and established model	39
Figure 4-1 Inheritance and inclusion structure of major classes	45
Figure 4-2 Class access relationship with the Analyzer	46
Figure 4-3 Main view of the developed program	47
Figure 4-4 Sub-dialog interfaces for inputting parameter figures	48
Figure 4-5 Total configuration process of the developed program.....	49
Figure 4-6 Main routine of Analyzer class	50
Figure 4-7 Function for obtaining the moment-curvature interaction.	51
Figure 4-8 Function for obtaining the P-M interaction.	51
Figure 4-9 Tendon configuration	53
Figure 4-10 Main routine of Analyzer class with unbonded tendons..	54
Figure 4-11 Sub-routine for calculating ultimate moment with unbonded tendons	54
Figure 4-12 Sub-routine for calculating moment-curvature relationship with unbonded tendons	55
Figure 4-13 Charts in the result dialog	57
Figure 5-1 Virtual machine environment for using BIAx.....	62
Figure 5-2 Sample 1: Cross section of unconfined concrete section...	64
Figure 5-3 Sample 1: Concrete material model	65
Figure 5-4 Sample 1: Steel material model	65

Figure 5-5 Sample 1: Mesh generation.....	66
Figure 5-6 Sample 1: Moment-curvature comparison.....	66
Figure 5-7 Sample 1: P-M interaction comparison.....	67
Figure 5-8 Sample 2: Cross section of confined concrete section.....	68
Figure 5-9 Sample 2: Unconfined and confined concrete models.....	68
Figure 5-10 Sample 2: Mesh generation.....	69
Figure 5-11 Sample 2: Moment-curvature comparison.....	70
Figure 5-12 Sample 2: P-M interaction comparison.....	70
Figure 5-13 Sample 3: Cross section of bonded prestressed concrete section.....	71
Figure 5-14 Sample 3: Concrete model.....	72
Figure 5-15 Sample 3: Tendon model.....	72
Figure 5-16 Sample 3: Moment-curvature comparison.....	73
Figure 5-17 Tendon stress increase models.....	75
Figure 5-18 Case study 1: Cross section of unbonded prestressed concrete section.....	76
Figure 5-19 Case study 1: Moment-curvature relations.....	77
Figure 5-20 Case study 1: Tendon increase rate at each curvature.....	78
Figure 5-21 Case study 2: Cross section of unbonded prestressed concrete section.....	80
Figure 5-22 Case Study 2: Moment-curvature relations.....	81
Figure 5-23 Case study 2: Tendon increase rate at each curvature.....	82
Figure A-1 Main window.....	90
Figure A-2 Supported material models and user interface.....	95
Figure A-3 Supported sectional shape and user interface when defining new section.....	96
Figure A-4 User interface for arranging rebars.....	97
Figure A-5 User interface for arranging tendons.....	97
Figure A-6 User interface for arranging structural steel.....	98
Figure A-7 User interface for setting four corners of confined area....	98

Figure A-8 User interface for setting analysis options	99
Figure A-9 Window for displaying analysis progresses	99
Figure A-10 Result window for moment-curvature relation	100
Figure A-11 Result window for P-M interaction	100

List of Symbols

a	Defined parameter of Yang et al. (2014) unconfined concrete model
A_1	Defined parameter of Yang et al. (2014) unconfined concrete model
A_s	Cross-sectional area of transverse reinforcement, mm ²
A_{sp}	Cross-sectional area of confined core, mm ²
b	Defined parameter of Yang et al. (2014) unconfined concrete model
b_{cx}	Core dimension for x direction, mm
b_{cy}	Core dimension for y direction, mm
d_s	Confined core diameter, mm
E_c	Elastic modulus of concrete, MPa
E_{ps}	Elastic modulus of tendon, MPa
E_s	Elastic modulus of mild steel, MPa
f^*	Normalized stress
f_0	Constant influencing determining β_1 value for Yang et al. (2014) unconfined concrete model, 10 MPa
f_c	Concrete stress, MPa

f_c'	Unconfined concrete strength of material, MPa
f_{cc}'	Confined concrete strength, MPa
f_{le}	Equivalent uniform pressure, MPa
f_{lex}	Effective lateral pressure in x direction acting perpendicular to core dimension, MPa
f_{ley}	Effective lateral pressure in y direction acting perpendicular to core dimension, MPa
f_{lx}	Lateral pressure from x direction, MPa
f_{ly}	Lateral pressure from y direction, MPa
f_{ps}	Tendon stress, MPa
f_{pu}	Tensile strength of tendon, MPa
f_{py}	Yield strength of tendon, MPa
f_s	Mild steel stress, MPa
f_y	Yield strength of mild steel, MPa
f_{yh}	Yield strength of transverse reinforcement, MPa
f_{yt}	Yield strength of transverse reinforcement, MPa
h''	Width of concrete core measured outside to outside of peripheral hoop, mm
K	Stress increase factor
K	Coefficient parameter determined by k_1 , f_{le} , and f_c'

K	Coefficient parameter for Ramberg-Osgood (1942) steel model
K	Coefficient constant for Mattock (1979) tendon model
k_1	Function of Poisson's ratio
k_{2x}	Coefficient for reducing pressure into effective lateral pressure of x direction
k_{2y}	Coefficient for reducing pressure into effective lateral pressure of y direction
M_t	Current normalized moment determined by normalized tendon stress increase
n	Exponent parameter for Ramberg-Osgood (1942) steel model
$n_{concrete}$	Parameter of normal concrete determined by strength for Popovics (1973) concrete model
n_{mortar}	Parameter of mortar determined by strength for Popovics (1973) concrete model
n_{paste}	Constant of concrete paste for Popovics (1973) concrete model
R	Constant influencing curve shape for Menegotto-Pinto (1973) steel model
r_i	Difference between point (x_i, y_i) and trendline derived by the least square method
s	Spiral spacing, mm
S	Summation of squared residual (r_i)
s_e	Unsupported transverse reinforcement length in each direction, mm
s_h	Center-to-center spacing of hoop sets, mm
$W(x)$	Lambert W function

w_0	Unit normal concrete weight (= 2300 kg/m ³)
w_c	Concrete density, kg/m ³
x_i	x coordinate value of experimental data
y_i	y coordinate value of experimental data
Z_m	Stress reduction slope in the range after maximum stress
β	Exponent coefficient parameter of tendon stress increase model
β_1	Defined key parameter of Yang et al. (2014) unconfined concrete model
Δf_{np}	Normalized tendon stress increase
ε^*	Normalized strain
ε_l	Confined concrete strain at maximum stress
ε_c	Concrete strain
ε_{c85}	Strain at 85% strength after maximum stress
ε_{co}	Concrete strain at maximum stress
ε_{cu}	Ultimate concrete strain
ε_{ps}	Tendon strain
ε_{pu}	Strain at tensile failure of tendon
ε_s	Mild steel strain

ε_y	Yield strain of mild steel
ρ	Transverse reinforcement ratio
ρ_s	Ratio of volume of hoop reinforcement to volume of concrete core measured outside to outside of hoops

Chapter 1. Introduction

After Eugène Freyssinet put the idea of prestressed concrete in practice in the 1930s, prestressing has become one of the most important reinforcement methods for concrete elements (Marrey and Grote, 2003). By reducing tensile stress of concrete with tensioned steel (as shown in **Figure 1-1**), prestressed concrete makes structural elements more durable even with less steel reinforcements. In addition, prestressed concrete is able to establish a large span of beams and slabs so that the material can be saved.

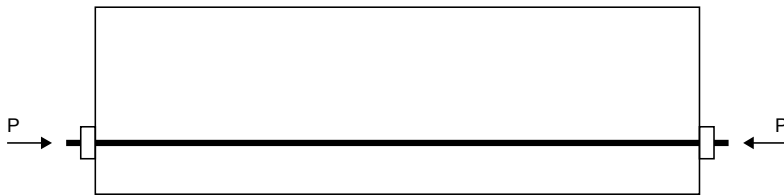


Figure 1-1 Longitudinal cross section of prestressed concrete

However, the research for analyzing the sectional behavior of a prestressed concrete element has not been thorough yet. Most of the commercial nonlinear finite element analysis programs for frames only support the non-prestressed elements. Although researchers are currently attempting to model three dimensional prestressed elements with general purpose finite element analysis programs, the computational cost needed for application in nonlinear finite element analysis programs for frames is too great.

If 3D finite element method is used to research only one prestressed concrete member in detail, then the method could be useful. However, excessive computing power will be necessary when researching an entire building with prestressed elements using the 3D finite element method.

Therefore, plastic hinge modeling (**Figure 1-2**) maybe necessary when

analyzing an entire building with prestressed elements and performing the displacement-based seismic design. Some of the previous sectional analysis programs has features of calculating the backbone curve of a variety of plastic hinges, but still is not equipped for prestressed elements.

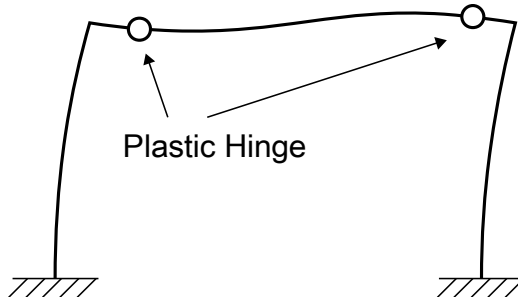


Figure 1-2 Plastic hinge of structural element

In this thesis, a new analytic model and computer program simplifies the analysis of an unbonded, post-tensioned, reinforced concrete element that enhances the efficiency. For the new analytic model, experiment data are collated. Several experimental data show that tendon stress increase has a certain relationship with the load or moment of the specimens. The new equation is set to be assigned to the program to analyze the unbonded post-tensioned element.

The program does not cover only prestressed elements, but also supports any reinforced concrete elements. The program makes users easy to perform the analysis, giving various features. The program is developed for the purpose of combining various material models and analytical methods which can be used for sectional analysis, contributing to the brand-new plastic hinge modeling of prestressed concrete elements.

Chapter 2. Review of Previous Studies

2.1 Design Code

The reinforced concrete design follows ACI 318-14 and KCI 2012 in normal situations. To calculate the nominal strength and design elements, several rules have been assumed since the ACI 318 Building Code was released. In this study, the new developed program is mainly designed to calculate the moment-curvature interaction and P-M interaction, which are generally in line with ACI 318-14 and KCI 2012.

At first, ACI 318 provides some assumptions for calculating each interaction. The force equilibrium and strain compatibility for the section are supposed to come before all else. Force equilibrium refers to when the sum of all forces loaded on a cross section are zero. The strain compatibility means that the strain value is directly proportional to the distance from the neutral axis. The assumptions must be satisfied for all calculations based on the cross-sectional information. **Figure 2-1** describes the assumptions in detail, where d is effective depth, c is the depth of compressive area and ϵ_{cu} is ultimate strain.

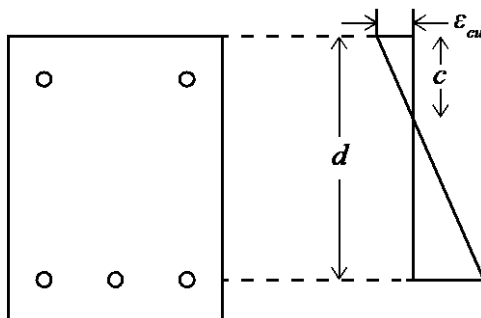


Figure 2-1 Strain compatibility description

There is one exception to this assumption: in the case of prestressed concrete,

the bonded or unbonded reinforcement has the prestressing strain.

Furthermore, the ultimate strain of concrete is assumed to be 0.003 and the tensile strength is neglected in the calculations. The stress in the compression zone can be considered the same as $0.85f_c'$ when distributed uniformly, as expressed in **Figure 2-2**, where f_c' is the concrete compressive strength. However, this assumption was made for easier calculation. In this study, the purpose is to develop a new computer program that can handle complex calculations, so this assumption can be elaborated and more accurate direct calculation can be made.

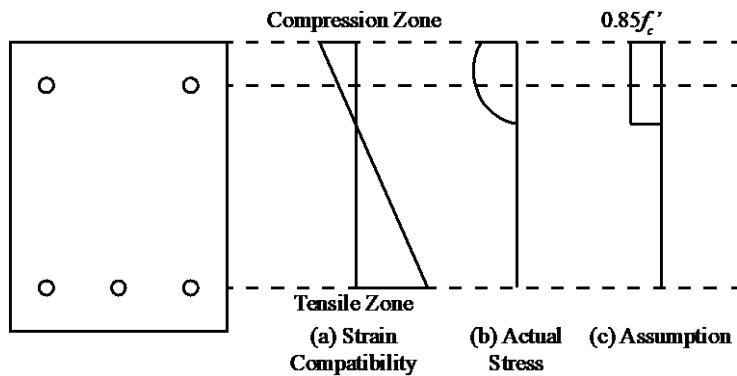


Figure 2-2 Compression zone approximation

2.2 Previous Studies

In order to calculate the moment-curvature and P-M interactions, the material model is necessary, which shows how the compressive and tensile stresses are distributed for the given strain. The new program, which is to be developed in this study, is based on several material models for calculating stress-strain relations. In this chapter, the material models are reviewed in order to use them appropriately in the program.

2.2.1 Concrete material models

Many concrete material models provide the stress-strain curve only in the negative strain range (i.e., compressive strain). According to the ACI 318 Building Codes, the tensile strength of concrete is neglected as well. In this thesis, concrete tension models are not included.

Concrete material models are made up of two major categories: unconfined concrete and confined concrete. Confined concrete is when concrete is reinforced by the transverse reinforcements that resist against the force perpendicular to the axial load. Unconfined concrete is the normal concrete with no transverse reinforcement. The former usually has better strength than unconfined concrete due to the restrained effect.

The following sections review the unconfined and confined concrete models to be used in the developed program where the parameters and formulas for the stress-strain curve are highlighted. All formulas are unified in the SI unit.

2.2.1.1 Hognestad (1951) confined concrete model

Hognestad (1951) proposed the stress-strain equation for confined concrete members. In Hognestad's study, the confined concrete column was tested. The eccentric load was given to the two different columns where one had a rectangular cross section and the other had a circular cross section. By analyzing the experimental results, the empirical equation is proposed.

The equation is made up of two parts: parabolic and linear. The parabolic ascending part is expressed as:

$$f_c = f_c' \times \left[2 \frac{\varepsilon_c}{\varepsilon_{co}} - \left(\frac{\varepsilon_c}{\varepsilon_{co}} \right)^2 \right] \quad (2-1)$$

where f_c is the concrete stress, f_c' is the original unconfined concrete strength, ε_c is the concrete strain, and ε_{co} is the strain at maximum stress.

The parabolic ascending part is established in the strain range from 0 to ε_{co} . At a strain larger than ε_{co} , the stress value decreases linearly in the range from ε_{co} to ε_{cu} as:

$$f_c = f_c' \times \left[1 - 0.15 \frac{\varepsilon_c - \varepsilon_{co}}{\varepsilon_{cu} - \varepsilon_{co}} \right] \quad (2-2)$$

where ε_{cu} is the ultimate concrete strain set at 0.0038, according to the study.

The stress-strain diagram by Hognestad (1951) is shown in **Figure 2-3**.

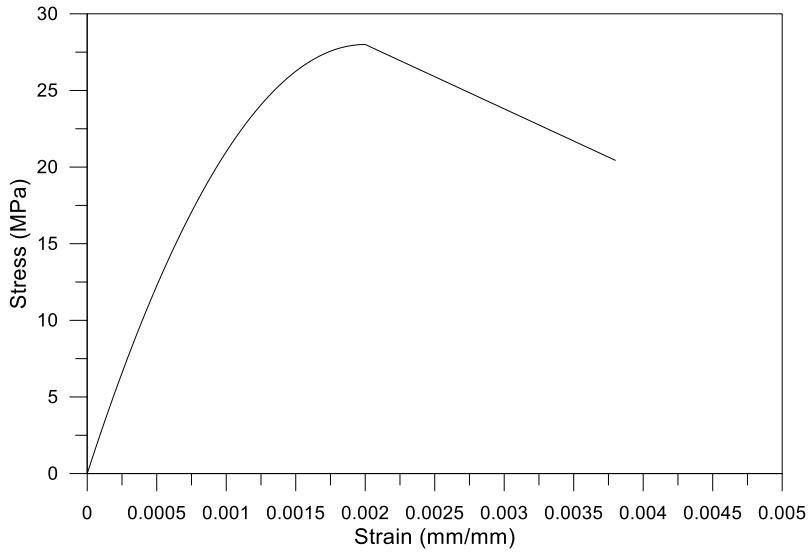


Figure 2-3 Normal concrete (28 MPa) stress-strain diagram by Hognestad confined concrete model

2.2.1.2 Modified Kent and Park concrete model

Kent and Park (1971) proposed the material model for unconfined and confined concrete where parabolic ascending and linear descending ranges exist similar to the Hognestad concrete model. The Kent and Park concrete model selected the Hognestad stress-strain equation for the parabolic range and made it compatible with both unconfined and confined concrete. However, this model does not describe the confined state well. Park et al. (1982) provided the modified Kent and Park concrete model. The modified model is more focused on describing the accurate stress-strain relation of confined concrete.

In the strain range from 0 to $0.002K$, a parabolic equation, Eq. (2-3), is utilized.

$$f_c = Kf_c' \left[2 \left(\frac{\varepsilon_c}{0.002K} \right) - \left(\frac{\varepsilon_c}{0.002K} \right)^2 \right] \quad (2-3)$$

For the strain range over $0.002K$,

$$f_c = Kf_c' [1 - Z_m (\varepsilon_c - 0.002K)] \quad (2-4)$$

where

$$K = 1 + \frac{\rho_s f_{yh}}{f_c'} \quad (2-5)$$

$$Z_m = \frac{0.5}{\frac{3 + 0.29f_c'}{145f_c' - 1000} + \frac{3}{4} \rho_s \sqrt{\frac{h''}{s_h}} - 0.002K} \quad (2-6)$$

where f_{yh} is yield strength of hoop reinforcement, ρ_s is ratio of volume of hoop reinforcement to volume of concrete core measured to outside of the hoops, h''

= width of concrete core measured to outside of the peripheral hoop and s_h = center-to-center spacing of hoop sets.

If the strain rate is high, a factor, 1.25, should be multiplied to the peak stress. Accordingly, Eq. (2-5) and Eq. (2-6) are changed to the following equations, respectively:

$$K = 1.25 \left(1 + \frac{\rho_s f_{yh}}{f_c'} \right) \quad (2-7)$$

$$Z_m = \frac{0.625}{\frac{3 + 0.29 f_c'}{145 f_c' - 1000} + \frac{3}{4} \rho_s \sqrt{\frac{h''}{s_h}} - 0.002 K} \quad (2-8)$$

Finally, the residual strength stress exists below a certain level. After descending post-ultimate stress stage, the residual strength remains at the following value:

$$f_c = 0.2 K f_c' \quad (2-9)$$

The stress-strain diagram for the modified Kent and Park concrete model is shown in **Figure 2-4**.

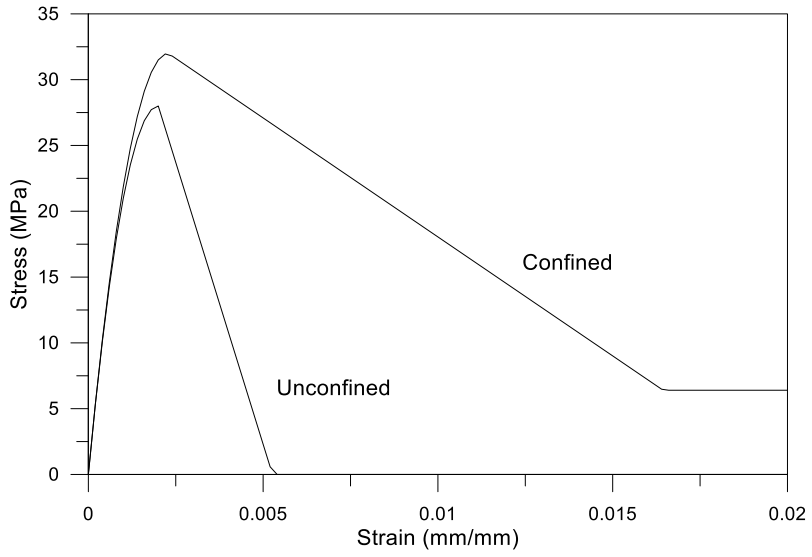


Figure 2-4 Normal concrete (28 MPa) stress-strain diagram by modified Kent and Park concrete model

2.2.1.3 Popovics (1973) unconfined concrete model

Popovics (1973) made an equation from his previous works for establishing the stress-strain diagram. Through curve-fitting relative stress-strain curves of various concretes (i.e. normal concrete, mortar, paste, etc.), the following formula is established:

$$f_c = f_c' \left(\frac{\varepsilon_c}{\varepsilon_{co}} \right) \left[\frac{n}{n-1 + (\varepsilon_c / \varepsilon_{co})^n} \right] \quad (2-10)$$

where the n parameter is defined as :

$$n_{concrete} = 58 \times 10^{-3} f_c' + 1.0 \quad (2-11)$$

$$n_{mortar} = 21.75 \times 10^{-3} f_c' + 1.5 \quad (2-12)$$

$$n_{paste} = 12 \quad (2-13)$$

The stress-strain diagram of the Popovics concrete model is shown in **Figure 2-5**.

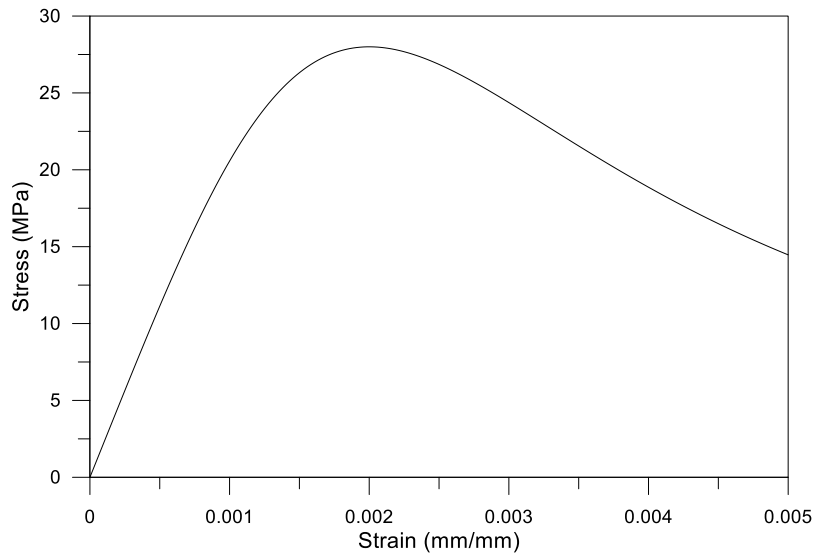


Figure 2-5 Normal concrete (28 MPa) stress-strain diagram by Popovics unconfined concrete model

2.2.1.4 Saatcioglu and Razvi (1992) confined concrete model

Saatcioglu and Razvi (1992) proposed a new way to predict the stress-strain relation of confined concrete that supports several types of transverse reinforcements, unlike with the modified Kent and Park confined concrete model. This particular model is verified by comparing with experimental results from Mander et al. (1988). The confined concrete model by Saatcioglu and Razvi (1992) has complex formulas for the stress-strain diagram.

The equations are shown as:

$$f_c = f_{cc}' \left[2 \left(\frac{\varepsilon_c}{\varepsilon_1} \right) - \left(\frac{\varepsilon_c}{\varepsilon_1} \right)^2 \right]^{\frac{1}{1+2K}} \leq f_{cc}' \quad (2-14)$$

$$f_c = f_{cc}' + 0.15 f_{cc}' \left(\frac{\varepsilon_c - \varepsilon_1}{\varepsilon_1 - \varepsilon_{c85}} \right) \quad (2-15)$$

where f_{cc}' is the confined concrete strength, ε_1 is the peak strain of confined concrete strength, ε_{c85} is the strain at 85% strength after peak maximum stress, and K is a coefficient parameter. These parameters are defined as:

$$f_{cc}' = f_c' + k_1 f_{le} \quad (2-16)$$

$$\varepsilon_1 = \varepsilon_{co} (1 + 5K) \quad (2-17)$$

$$K = \frac{k_1 f_{le}}{f_c'} \quad (2-18)$$

$$\varepsilon_{c85} = 260 \rho \varepsilon_1 + 0.0038 \quad (2-19)$$

where f_c' is the normal concrete strength before confinement, k_1 is a function of Poisson's ratio, f_{le} is the equivalent uniform pressure, and ρ is the transverse

reinforcement ratio. Among these parameters, k_1 is defined as:

$$k_1 = \frac{6.7}{f_{le}^{0.17}} \quad (2-20)$$

The equivalent uniform pressure and transverse reinforcement ratio are determined by the yield strength of transverse reinforcements and rebar's arrangement. Thus, the ρ and f_{le} values are defined as:

$$\rho = \frac{\Sigma A_s}{s(b_{cx} + b_{cy})} \quad (2-21)$$

$$f_{le} = \frac{f_{lex}b_{cx} + f_{ley}b_{cy}}{b_{cx} + b_{cy}} \quad (2-22)$$

$$f_{le} = \frac{2A_{sp}f_y}{d_s s} \quad (2-23)$$

where A_s is the total area of transverse reinforcement in both directions, b_{cx} and b_{cy} are the core dimensions for each direction, f_{lex} and f_{ley} are the effective lateral pressures acting perpendicular to core dimensions, A_{sp} is the cross-sectional area of the confined core, f_y is the yield strength of transverse reinforcement, d_s is the confined core diameter, and s is the spiral spacing. **Eq. (2-22)** and **Eq. (2-23)** are for the rectangular-shaped confined core and spiral confined core, respectively. The effective lateral pressure for each direction (f_{lex}, f_{ley}) is defined as:

$$f_{lex} = k_{2x}f_{lx} \quad (2-24)$$

$$f_{ley} = k_{2y}f_{ly} \quad (2-25)$$

where f_{lx} and f_{ly} are lateral pressures from each direction, and k_{2x} and k_{2y} are

coefficients for reducing the pressure into effective lateral pressures. The lateral pressure and reducing coefficients are derived by:

$$f_l = \frac{\Sigma A_s f_{yt} \sin a}{s b_c} \quad (2-26)$$

$$k_2 = 0.26 \sqrt{\frac{b_{cx} b_{cy}}{s s_e f_l}} \leq 1.0 \quad (2-27)$$

where A_s is the cross-sectional area of transverse reinforcement, f_{yt} is the yield strength of transverse reinforcement, a is the angle between lateral pressure direction and transverse reinforcement direction, b_c is the core width of each direction, b_{cx} and b_{cy} are the core width in the x and y directions, respectively, s is the spacing of transverse reinforcement, and s_e is the unsupported transverse reinforcement length in each direction.

Finally, the residual strength stress exists below a certain level. After descending post-ultimate stress stage, the residual strength remains at the following value:

$$f_c = 0.2 K f_{cc}' \quad (2-28)$$

According to the expressions, the Saatcioglu and Razvi confined concrete model is based on actual specimen information. Assuming that there is an example specimen whose height and width of the core are 400 mm and with 28 MPa normal concrete material that is reinforced by 4 D22 rebars and confined by 400-MPa-strength D15 transverse hoops at every 100 mm, the confined concrete area has the stress-strain relationship shown in **Figure 2-6**.

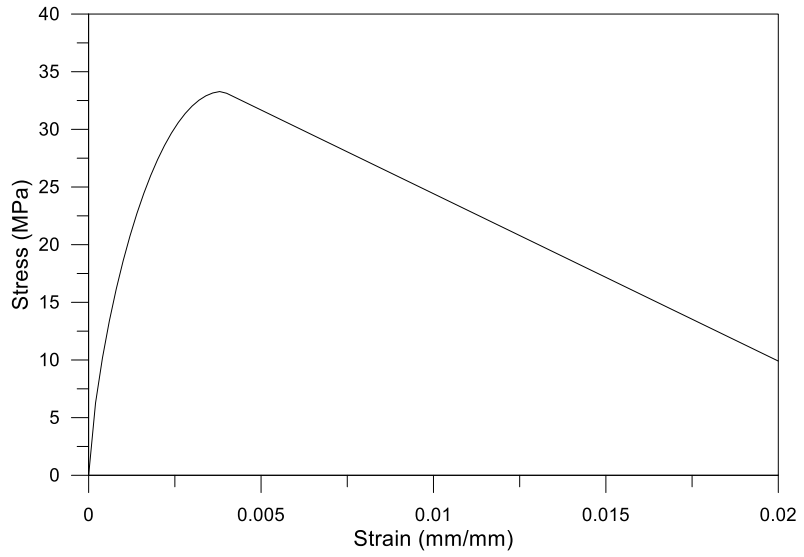


Figure 2-6 Normal concrete (28 MPa) stress-strain diagram by Saatcioglu and Razvi model

2.2.1.5 Yang et al. (2014) unconfined concrete model

The unconfined concrete model developed by Yang et al. (2014) focuses on coping with various types of concrete. In this study, concrete compressive strength and concrete density are selected as important parameters. In particular, the accurate stress-strain line curve is obtained for the larger parameters. This model is expressed as:

$$f_c = \left(\frac{(\beta_1 + 1) \left(\frac{\varepsilon_c}{\varepsilon_0} \right)}{\left(\frac{\varepsilon_c}{\varepsilon_0} \right)^{\beta_1 + 1} + \beta_1} \right) f_c' \quad (2-29)$$

where β_1 is the defined key parameter and ε_0 is the strain at maximum stress. Each parameter is defined as:

$$\varepsilon_0 = 0.0016 \exp \left(240 \left(\frac{f_c'}{E_c} \right) \right) \quad (2-30)$$

$$\beta_1 = 0.2 \exp \left(0.73 \left(\frac{f_c'}{f_0} \right)^{0.67} \left(\frac{w_0}{w_c} \right)^{1.17} \right) \quad \text{when } \varepsilon_c \leq \varepsilon_0 \quad (2-31)$$

$$\beta_1 = 0.41 \exp \left(0.77 \left(\frac{f_c'}{f_0} \right)^{0.67} \left(\frac{w_0}{w_c} \right)^{1.17} \right) \quad \text{when } \varepsilon_c > \varepsilon_0 \quad (2-32)$$

where E_c is the modulus of elasticity, f_0 is 10 MPa, w_c is the concrete density, and w_0 is 2300 kg/m³. The modulus of elasticity in this study is formulated as:

$$E_c = A_1 (f_c')^a \left(\frac{w_c}{w_0} \right)^b \quad (\text{MPa}) \quad (2-33)$$

where A_1 , a , and b are the defined parameters in this study best fit at 8470, 1/3,

and 1.17, respectively.

According to the study, this unconfined concrete model fits well when compared to the experimental results on compressive strength that ranges from 8.4 to 170 MPa with a density ranging from 1,200 to 4,500 kg/m³.

Assuming that there is an 80 MPa 2300 kg/m³ concrete material, the stress-strain diagram is determined as shown in **Figure 2-7**.

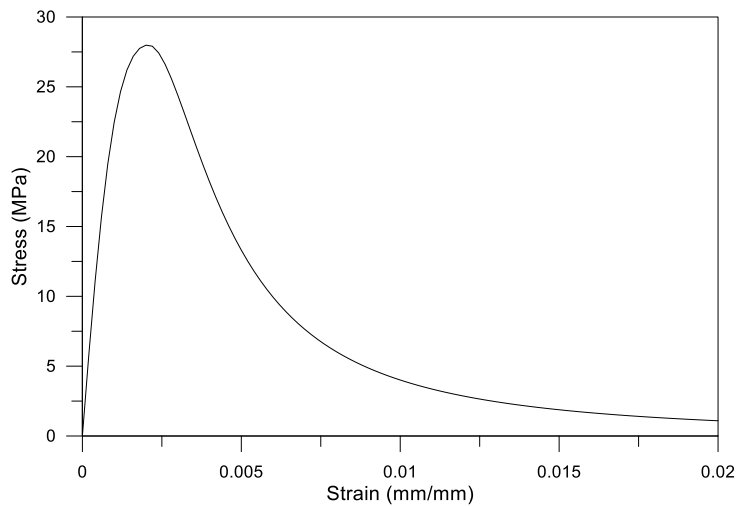


Figure 2-7 Normal concrete (28 MPa) stress-strain diagram by Yang et al. unconfined concrete model

2.2.2 Steel material models

A steel material model is necessary for rebars and extra steel reinforcement (e.g. SRC). Unlike concrete material models, steel material models have stress-strain curves in both compressive and tensile strain ranges. The symmetric stress-strain curves for each steel model are usually drawn as the symmetrical figure with respect to the zero point.

Another characteristic of steel material models, compared to concrete material models, is the infinitely increasing or staying stress value depending on strain. Steel has much larger ultimate strength and ultimate strain compared to concrete. The ultimate strength and strain of steel is not considered for design in ACI 318-14.

The following sections review steel models to be used in the developed program. The parameters and formulas for the stress-strain curve are highlighted for review.

2.2.2.1 Bilinear steel model

The Bilinear steel model has been used frequently as it is simple and corresponds well with experimental results. The model is made up of two parts depending on the yield state. The model is established by:

$$f_s = E_s \varepsilon_s \leq f_y \quad (2-34)$$

$$f_s = E_s a(\varepsilon_s - \varepsilon_y) + f_y > f_y \quad (2-35)$$

where f_s is the steel stress, E_s is the elastic modulus of steel, ε_s is the steel strain, f_y is the steel yield strength, a is stress hardening factor, and ε_y is the steel yield strain.

The example of 400 MPa steel rebar stress-strain diagram is shown in **Figure 2-8**.

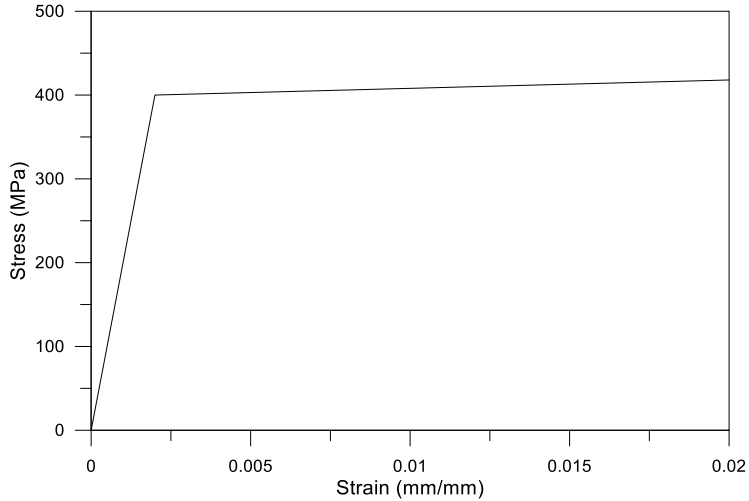


Figure 2-8 400 MPa steel rebar stress-strain diagram by bilinear model

2.2.2.2 Ramberg-Osgood (1943) steel model

The Ramberg-Osgood (1943) steel model proposed a smooth equation. In their study, it was mentioned that the previous method for describing the stress-strain curve of steel is not appropriate for efficiently designing the member. For example, the bilinear model has a very simple expression, while the Ramberg-Osgood model provides a more delicate equation expressed as:

$$\varepsilon_s = \frac{f_s}{E_s} + K \left(\frac{f_s}{E_s} \right)^n \quad (2-36)$$

where ε_s is the steel strain, f_s is the steel stress, E_s is the elastic modulus of steel, and K and n are the constants. The K is calculated from

$$K \left(\frac{f_s}{E_s} \right)^n = \alpha \left(\frac{f_s}{E_s} \right) \left(\frac{f_s}{f_y} \right)^{n-1} \quad (2-37)$$

where f_y is the yield strength of steel and α is the constant. Eq. (2-36) can be rewritten by plugging Eq. (2-37) into Eq. (2-36) as:

$$\varepsilon_s = \frac{f_s}{E_s} + \alpha \left(\frac{f_s}{E_s} \right) \left(\frac{f_s}{f_y} \right)^{n-1} \quad (2-38)$$

In **Eq. (2-38)**, $\alpha \left(\frac{f_s}{E_s} \right)$ is considered as the yield offset. The constant n plays a role in controlling how smooth the knee-part is, and the stress-strain diagram is shown in **Figure 2-9** to describe an example model when the strength, yield offset, and n value are 400 MPa, 0.002, and 10, respectively.

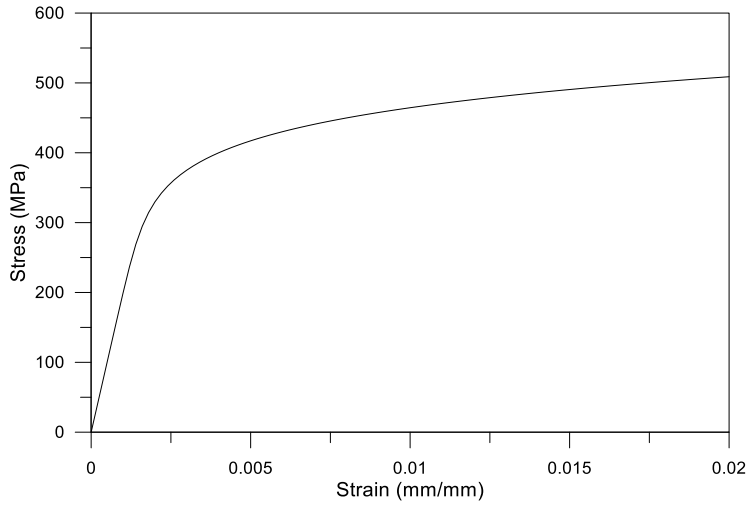


Figure 2-9 400 MPa steel rebar stress-strain diagram by Ramberg-Osgood model

2.2.2.3 Menegotto-Pinto steel model

Menegotto and Pinto (1973) proposed a revised stress-strain equation designed to describe the cyclic behavior of the material, but the first cycle can be used as a stress-strain curve model. The stress-strain equation is described with normalized stress and strain variables like:

$$f^* = \frac{\varepsilon^*}{\left(1 + \varepsilon^{*R}\right)^{\frac{1}{R}}} \quad (2-39)$$

where f^* is the normalized stress, ε^* is the normalized strain, and R is the constant influencing the curve shape. The normalized stress and strain can be expressed by:

$$f^* = \frac{f_s}{f_y} \quad (2-40)$$

$$\varepsilon^* = \frac{\varepsilon_s}{\varepsilon_y} \quad (2-41)$$

The model has other equations for expressing cyclic behavior besides **Eq. (2-39)**. However, only the stress-strain backbone is reviewed in this thesis.

The stress-strain diagram by the model is shown in **Figure 2-10** to show an example when the strength, strain hardening ratio, and R value are 400 MPa, 0.005, and 10, respectively.

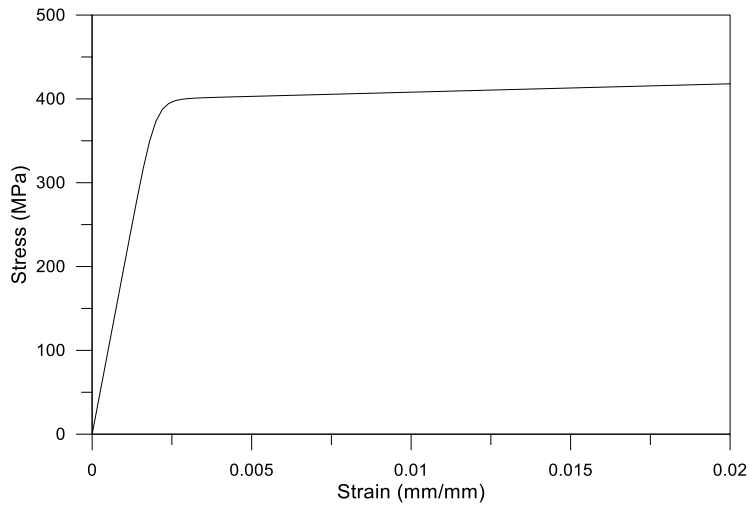


Figure 2-10 400 MPa steel rebar stress-strain diagram by Menegotto-Pinto model

2.2.3 Prestressing steel or tendon material model

The prestressing steel or tendon material model has a similar tendency as steel models, but the tendon has a much larger tensile strength than mild steel material model. Regardless of bonded or unbonded condition, the same material model is used.

In the case of bonded tendons, the strain behavior follows the strain compatibility assumption of the ACI 318 Building Code. In the case of unbonded tendons, the tendon is considered a tensile-only-member. The strain behavior is different from concrete or rebars, and is always in tension for various on the curvature changes. To solve this, the stress variation-moment relationship is newly developed according to the following section.

In addition, the tendon is made from steel as well, which means the elasticity modulus retains a similar value as mild steel models in the tendon model.

The following sections review the tendon models used in the developed program. The parameters and formulas for the backbone curve are highlighted for the reviews.

2.2.3.1 PCI tendon model

Precast/Prestressed Concrete Institute provides a tendon model in the publication called the PCI Design Handbook (2010). The tendon model is developed for two kinds of tendon strength: 250 ksi (approx. 1750 MPa) and 270 ksi (approx. 1860 MPa). The curves are defined separately.

Both tendon models have the same expression as the following for the elastic range:

$$f_{ps} = 196,479 \varepsilon_{ps} \quad (2-42)$$

where f_{ps} is the tendon stress and ε_{ps} is the tendon strain. After the elastic state, 250 ksi and 270 ksi tendon models are defined as in the following two equations, respectively:

$$f_{ps} = 6.894 \left(250 - \frac{0.04}{\varepsilon_{ps} - 0.0064} \right) \quad (2-43)$$

$$f_{ps} = 6.894 \left(270 - \frac{0.04}{\varepsilon_{ps} - 0.007} \right) \quad (2-44)$$

The stress-strain relationship of the PCI tendon model is given in **Figure 2-11**.

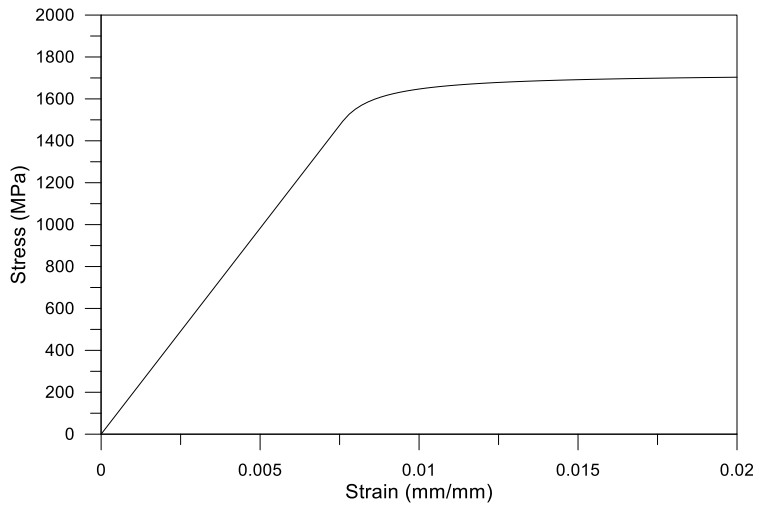


Figure 2-11 1750 MPa tendon stress-strain diagram by PCI tendon model

2.2.3.2 Mattock tendon model

Mattock (1979) proposed a modified stress-strain equation from Naaman (1977) based on the Menegotto-Pinto steel model. Mattock (1979) modified the original model in order to make it easy for small calculators to use. The stress-strain curve by Mattock model is as the following:

$$f_s = \varepsilon E \left[Q + \frac{1-Q}{\left\{ 1 + \left(\frac{\varepsilon E}{Kf_{py}} \right)^R \right\}^{1/R}} \right] \quad (2-45)$$

where

$$Q = \frac{f_{pu} - Kf_{py}}{\varepsilon_{pu} E - Kf_{py}} \quad (2-46)$$

where f_{pu} is the tensile strength of tendons, f_{py} is the yield strength of tendons, and K and R are coefficients. A reasonable K value for the seven-wire strands is 1.04. In addition, the R value can be determined by solving **Eq. (2-45)** and satisfying the following condition:

$$f_s = f_{py} \quad \text{when} \quad \varepsilon = 0.01 \quad (2-47)$$

The stress-strain diagram from the model is shown in **Figure 2-12**.

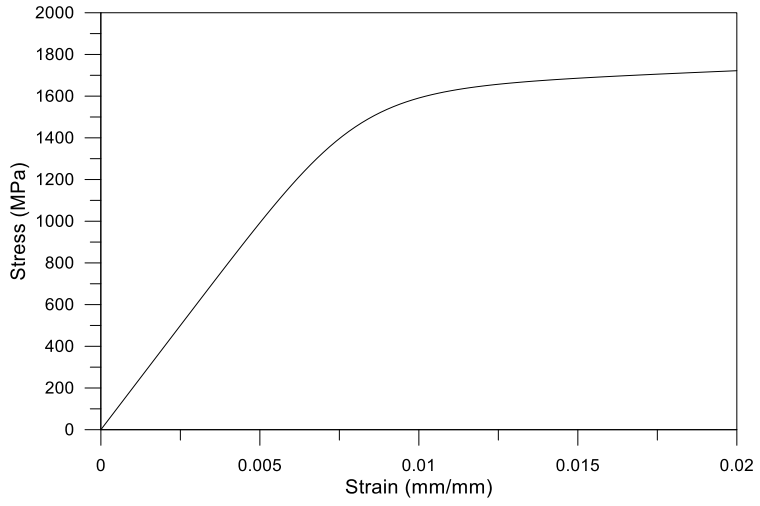


Figure 2-12 1860 MPa tendon stress-strain diagram by Mattock model

2.3 Summary

In this chapter, the structural assumptions and the material models used in the developed program are reviewed. The review is summarized as follows:

1. The basic structural assumption, such as force equilibrium and strain compatibility, should be used as a basis in the program according to ACI 318 and KCI 2012.
2. For each structural component (e.g. concrete, rebar and tendon), several representative material models are reviewed. All models present appropriate stress-strain curves.
3. As the only exception, unbonded prestressed concrete elements do not follow the strain compatibility since the unbonded tendon moves separately from the concrete.
4. Given that unbonded prestressed concrete elements are not in accordance with the strain compatibility, an additional way for describing the behavior of unbonded prestressed elements would be necessary.

Chapter 3. Experimental Data Assessment for Unbonded Post-Tensioned Members

For reinforced concrete element and pre-tensioned element with bonded tendons, moment-curvature relation and P-M interaction can be determined following the assumptions from ACI 318-14 Building Code and KCI 2012. Using the stress-strain model of materials, strain compatibility, and effective strain, the reasonable calculations can be carried out.

However, in the case of post-tensioned elements with unbonded tendons, this method cannot be used. The behavior of unbonded tendons follows the force equilibrium, but not the strain compatibility. Since the traditional method is not available for post-tensioned elements with unbonded tendons, a new method is needed.

In this chapter, the experimental data assessment for unbonded post-tensioned members is performed. Through the assessment of several experiments with various conditions, the empirical relation between the tendon stress increase and load is established.

3.1 Experimental Data

To simplify the unbonded post-tensioned concrete element analysis and enhance the efficiency, a new analytic model is needed. For the new analytic model, experiment data are collated. Several experimental data show that the tendon increase has a certain relationship with the load or moment of the specimens. The new equation is set up from the relationship and assigned to the program to analyze the unbonded post-tensioned element.

3.1.1 Foutch et al. (1990)

Foutch et al. (1990) performed the cyclic loading test for the post-tensioned slab. The specimens were tested under various conditions depending on the loading position and number of tendons. **Figure 3-1** shows the test results in the redrawn diagram by extracting the data in the inelastic stage.

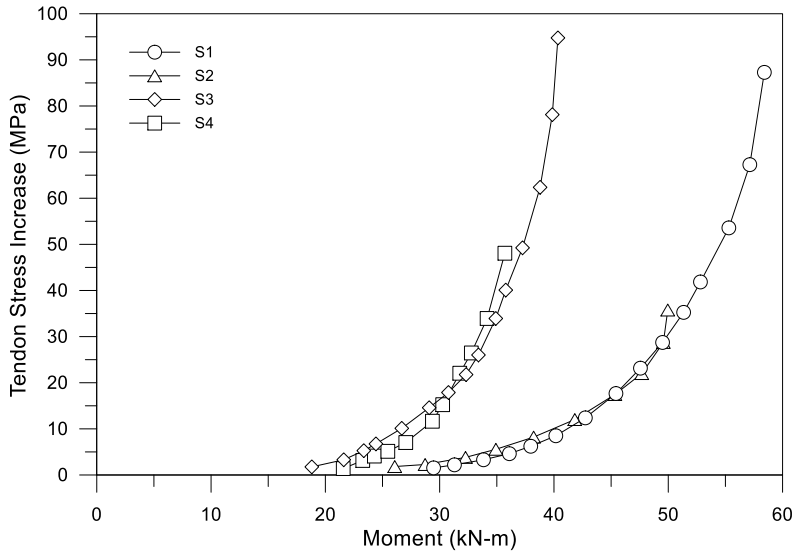


Figure 3-1 Experimental results from Foutch et al. (1990)

Specimens S1 and S2 had the same number of tendons, while S3 and S4 had the same number of tendons, but with smaller numbers than S1 and S2. The distance between the column and loading point for S1 and S2, S2 and S3, and S3 and S4 were about 1067, 610, and 305 mm, respectively. The diagram shows that the distance between the column and loading point increases the tendon stress while the number of tendons influences the maximum moment.

In addition, the diagram shows the exponential increment of tendon stress increases for the moment.

3.1.2 Lee et al. (2010)

Lee et al. (2010) performed loading tests for the post-tensioned 2-bay beams where the tendon for post-tensioning had the V-shaped profile. Thus, the test results are compared to the analysis results. Although there are a total of nine specimens for the experiment, Lee et al. (2010) provided only seven results on the relationship between the tendon stress increase and load. Among the given results, one is excluded due to its T-shaped cross section. **Figure 3-2** shows the tendon stress increase depending on the load.

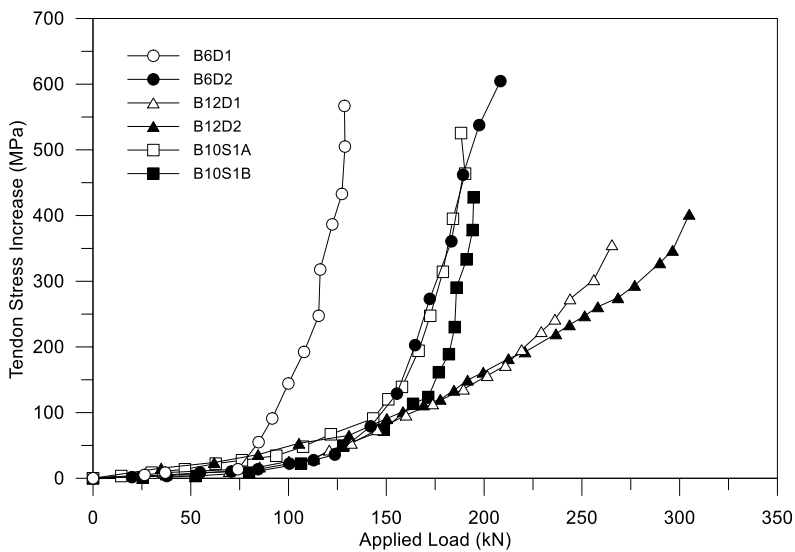


Figure 3-2 Experimental results from Lee et al. (2010)

From B6D1 to B10S1B, all specimens had different conditions according to the amount of rebars and tendons. Similar results to those in **Section 3.1.1** are observed. All data show the tendency for exponential increments. In particular, B6D2, B10S1A, and B10S1B exhibited almost the same tendon stress increments as the applied load. The data do not increase smoothly like those in **Section 3.1.1**, probably due to the experimental error.

3.1.3 Burns et al. (1978)

Burns et al. (1978) reported the behavior of the unbonded, post-tensioned, one-way slab with distributed load. The tendon stress increases and slab displacement increments were established according to the loads. Twenty specimens were used in the experiment, although only six specimens' results of tendon stress increases were provided as shown in **Figure 3-3**.

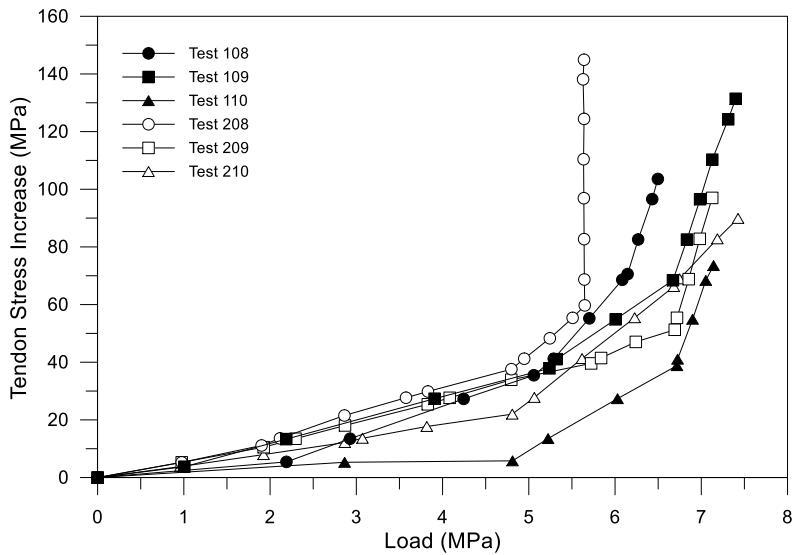


Figure 3-3 Experimental results from Burns et al. (1978)

As with the preceding experiments, the diagram shows a similar increment tendency. Unusually, Specimen Test 208 showed sudden increments at the 5.6 MPa distributed load.

3.1.4 Zhou and Zheng (2014)

Zhou and Zheng (2014) carried out the post-tensioned 2-bay continuous beam experiment with vertical point loads. A total of 16 specimens were used in the experiment and categorized into A, B, C, and D depending on the global reinforcement index and the controlled tensioning stress coefficient. **Figure 3-4** shows the results.

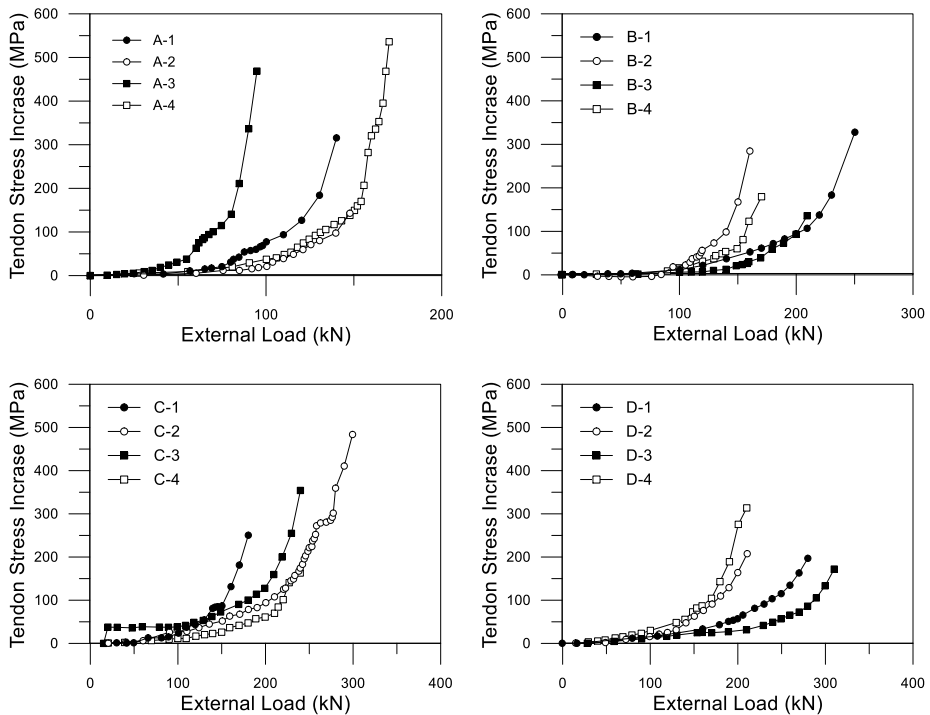


Figure 3-4 Experimental results from Zhou and Zheng (2014)

In essence, the specimens in A and C categories exhibited more tendon stress increases while those in B and D categories exhibited less. All diagrams show smoothly growing rates of tendon stress increase. For A-4 and C-2, the growing rate decreased suddenly before it increased again. Except for the anomaly, the diagrams look similar to aforementioned studies.

3.1.5 Tao and Du (1985)

Tao and Du (1985) performed post-tensioned 1-bay beam experiments with two point loads and straight profile tendons. There were 26 specimens with various conditions. Only the 9 specimens had the data of tendon stress change.

Figure 3-5 shows the recorded data.

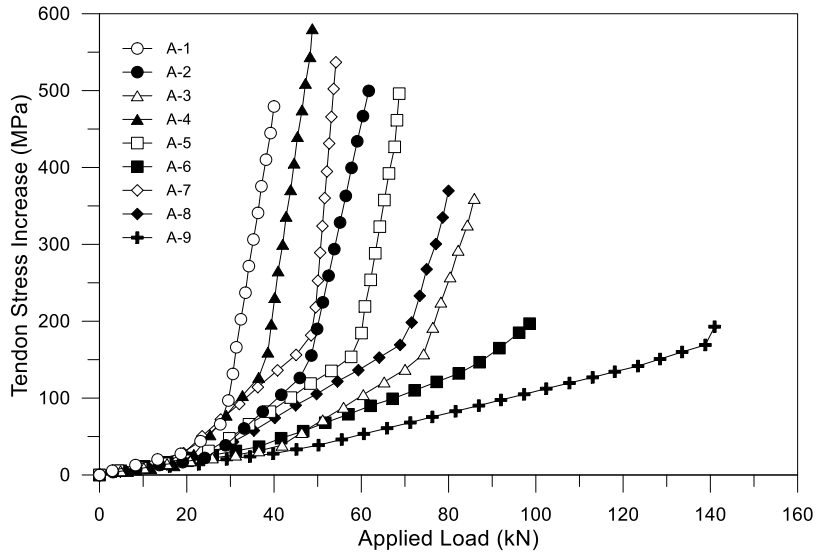


Figure 3-5 Experimental results from Tao and Du (1985)

In this study, the specimens experienced various amounts of tendon stress increases for increasing load. Unlike others, A-6 and A-9 had almost linear tendency while the yielding point of tendons was not clear.

3.1.6 Lim et al. (1999)

Lim et al. (1999) performed experimental examinations to determine if certain variables affect the behavior of unbonded tendons. There were a total of 14 specimens in this study categorized into seven groups (from A to G) according to effective stress, concrete strength, tendon cross-sectional area, etc. **Figure 3-6** shows the entire specimen load-tendon stress increase relations.

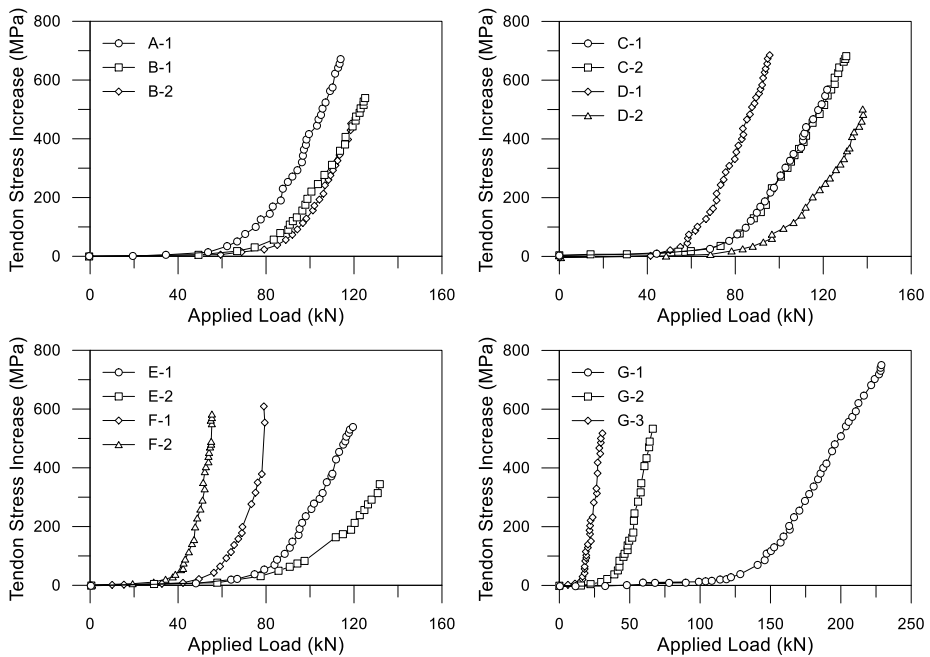


Figure 3-6 Experimental results from Lim et al. (1999)

The results are similar to the preceding results. Specimen G-3, whose aspect ratio was much larger than the others, had a much larger load than the other specimens at the ultimate state.

3.2 Empirical Model Development

When looking into the experimental data collectively, the tendon stress tends to increase by load or moment. The moment is defined as an expression of the physical quantity times the distance in the concept of physics. In other words, the moment has the linear relationship with the load. The experimental data show load or moment on x axis. Both of the load and moment can be normalized by each maximum figure.

Unlike the load or moment on x axis, the tendon stress increase on y axis just can be normalized by the maximum value without any other consideration. The normalized interaction is shown in **Figure 3-7**.

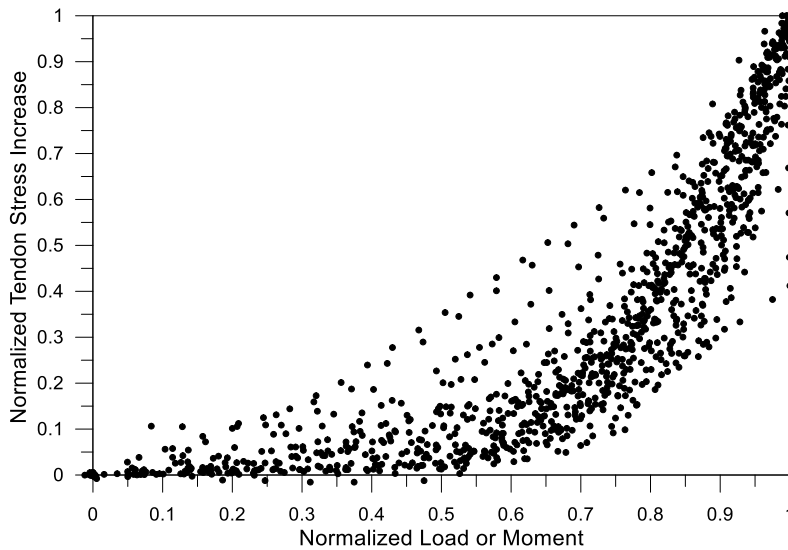


Figure 3-7 Interaction diagram of normalized tendon stress increase and normalized load or moment

The interaction of normalized tendon stress increase and load/moment is formalized through curve fitting utilizing the least square method believed to have been first developed by Carl Friedrich Gauss (1809). The method minimizes the S variable, which is the sum of squared residuals, in order to find the trend line.

$$S = \sum_{i=1}^n r_i^2 \quad (3-1)$$

The r_i variable is the difference between the original data and trend line, as defined in **Eq. (3-2)**.

$$r_i = y_i - f(x_i, \beta) \quad (3-2)$$

where x_i and y_i are the coordinate values from original data points and β is the coefficient for the trend line.

According to **Figure 3-7**, the data started at (0, 0) and finished at (1, 1). All experimental data shows the exponentially increasing tendency. Therefore, the basic trend line model can be set as **Eq. (3-3)**.

$$f(x_i, \beta) = xe^{\beta(x-1)} \quad (3-3)$$

After setting the model, the curve fitting calculation is performed using Matlab Curve Fitting Tool as shown in **Figure 3-8**.

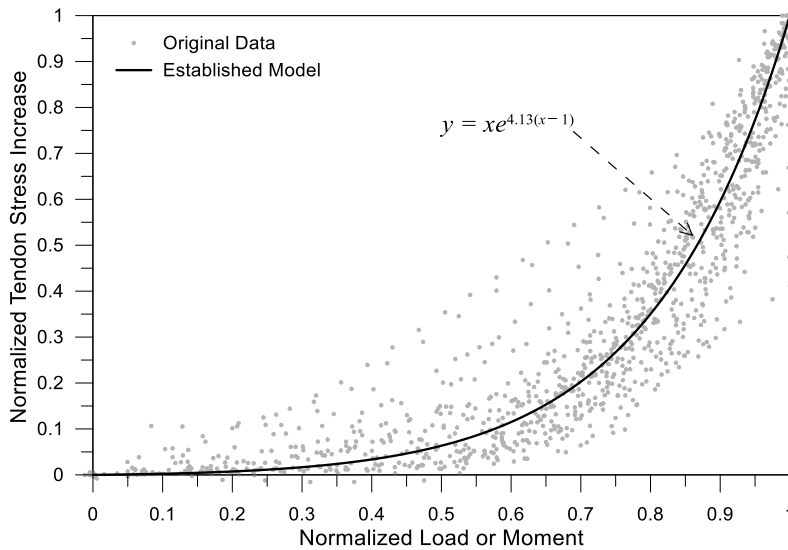


Figure 3-8 Normalized original experimental data and established model

The β value is drawn to 4.13 at 95% confidence bounds while the S value is calculated as 7.292.

The established model can now be used to calculate the unbonded PT element moment. When the program analyzes unbonded PT element, strain compatibility for other components except unbonded tendons is considered at first. Then the force equilibrium including unbonded tendons is checked. At last, the newly established relation model between tendon stress increase and load is used for determining how unbonded tendons should behave. The detailed explanation about the process is given in 0.

3.3 Summary

In this chapter, the prestressed concrete experiments with various conditions are reviewed and a new relationship between tendon stress increase and load/moment is established based on the evaluation of the previous experiments. The following is obtained from this chapter:

1. The experiments have different conditions, when it comes to the concrete strength, location and number of loading points, profile of tendons and so on. Most of the previous data shows a similar exponentially-increasing tendency between the tendon stress increase and load/moment, although some of the results show almost a linear tendency.
2. In order to describe the behavior of unbonded tendons, the relation between the tendon stress increase and load/moment of tendons is developed. Through curve-fitting process using the least square method, the relation is expressed as an exponential equation.

Chapter 4. Program Development

4.1 Purpose and Outline

The new program was developed to analyze the section of elements with various conditions. The goal of the program is to calculate and analyze every reinforced concrete member.

Microsoft Visual Studio 2017 was used to develop the program in an integrated development environment. Visual Studio is excellent for developing Windows applications written in C#, which is a programming language designed for object-oriented programming that can make the developing process fast, systematic, and easily expandable. Matlab and Python are not used in this study, because they do not have good features for establishing GUI (Graphical User Interface) although they are usually used for researching nowadays.

The developed program is designed so that users can conveniently input section data. A well-organized GUI can allow users to easily use the program.

4.2 Program Structures

Several programming strategies were utilized to develop the program. Since C# is an object-oriented programming language unlike C or Fortran, the program is well-structured to be expanded easily.

The program is made up of several classes bound together in the developed program as shown in **Table 4-1**. The classes are explained in the table with major roles in the program.

Table 4-1 Major class names and roles

Class	Role
IMaterial ^a	Define material model. (e.g. Modified Park and Kent Unconfined Concrete Model)
IShape ^a	Determine cross-sectional shape. (e.g. Square, Rectangular, Circle, T-shape, etc.)
IComponent ^a	Combine IMaterial and IShape into section components. (e.g. Concrete base, Rebar, Tendon, etc.)
Section	Make an entire section element. This class is made up of several IComponent instances.
Analyzer	Perform analyzing Section class instances.
ProjectManager	Control data in the Section class instances. Open and Save the project file (MCC file).

a. The prefix “I” refers to the abstract class or the interface according to the traditional naming protocol in the program code.

IMaterial, IShape, and IComponent have a lot of subclasses. For example, the concrete base class extends IComponent. The IComponent class must have the material model and shape. If there is a rectangular shaped concrete base modeled by Modified Kent and Park unconfined concrete model, they are realized through extending IShape and IMaterial.

The Section class holds all information about an entire section element. Basically, the Section class is a list of IComponent instances holding all the necessary methods for analysis by the Analyzer class. The Analyzer takes

essential data from the Section class and is calculated using the data. In every step, from defining the material model to analyzing the section, the ProjectManager class is involved in controlling the variables and project files. The section designs and final analysis results are saved into MCC files by the ProjectManager class.

Figure 4-1 shows how the major classes (shown in **Table 4-1**) and minor classes (not shown) are organized in the entire program.

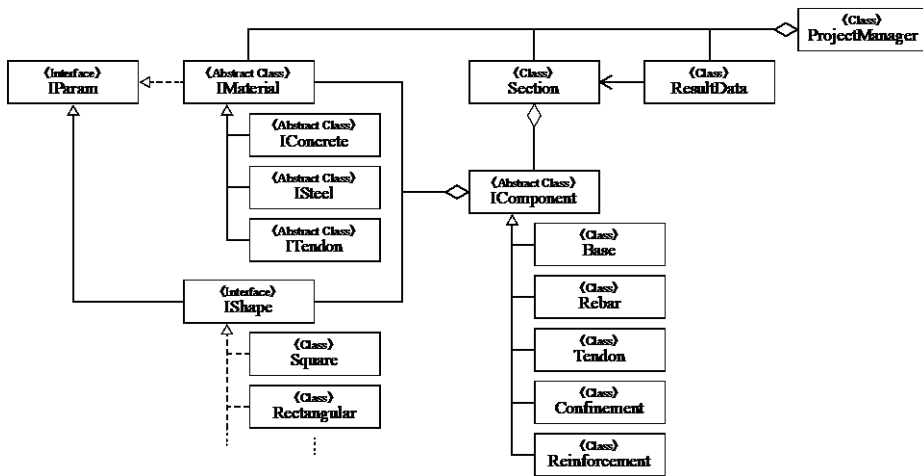


Figure 4-1 Inheritance and inclusion structure of major classes

The Analyzer class is excluded from **Figure 4-1**, because it can communicate with the ProjectManager in order to read and write data. The Analyzer class mainly consists of methods necessary for calculation rather than other data. In other words, it does not establish any kind of relationship with other major classes: inheritance or inclusion. Instead, the Analyzer class has some simple minor classes used for the calculation. The classes used in the Analyzer class are shown in **Figure 4-2**.

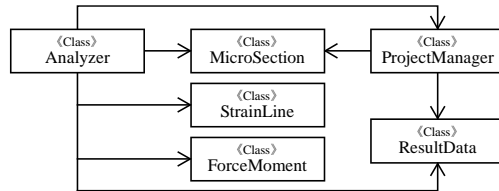


Figure 4-2 Class access relationship with the Analyzer

The Analyzer receives the list of MicroSection class instances from the ProjectManager and establishes the force equilibrium condition using StrainLine through trial and error. The MicroSection class instances are saved to ForceMoment class until the Analyzer receives the calculated results. The results are provided to the ProjectManager using ResultData class. The more detailed calculation process will be shown in the following sections.

4.3 Material and Section Configuration

The program consists of a main form and a result form. Each form has several sub-dialog interfaces for the program to interact with users. The main form shows components on the left side and cross-sectional diagram on the right side. The view for section components is built with the tree view, so a user can recognize the component hierarchy. **Figure 4-3** shows an example of the main view.

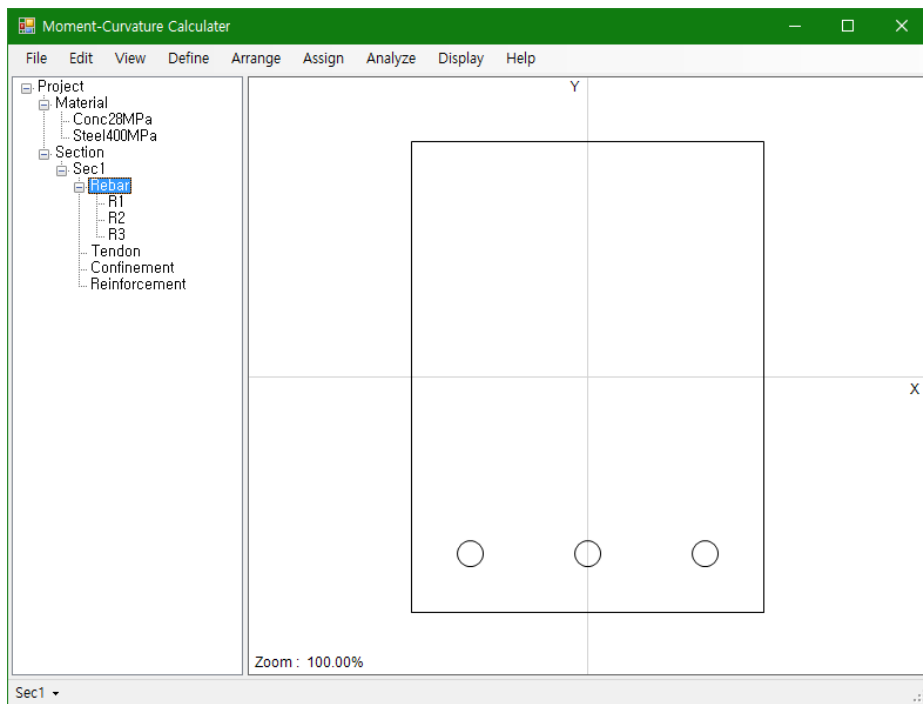
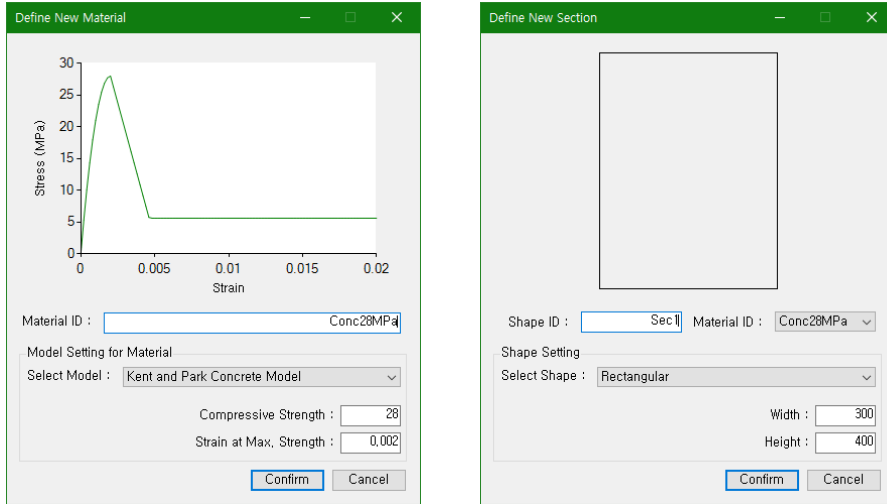


Figure 4-3 Main view of the developed program

The component hierarchy can be classified under Materials and Sections. Materials are the parameterized material models (e.g., Modified Kent and Park Unconfined Concrete Model, Bilinear Steel Model, and PSI Tendon Model) while Sections are the set of cross-sectional information. Each section item has sub-information on concrete base, rebars, tendons, confinements, and extra steel reinforcements (for steel reinforced concrete). The sub-information

is based on material models and additional parameters. **Figure 4-4** shows an example of sub-dialog interfaces, which is designed for conveniently inputting parameter figures and interacting with users.



(a) Material model configuration

(b) Concrete section configuration

Figure 4-4 Sub-dialog interfaces for inputting parameter figures

The total configuration process (including material model selection, parameter inputs, rebar arrangement, etc.) follows the flowchart shown in **Figure 4-5**. Material configuration and section configuration should be carried out in order. If the material information does not exist when the section is being set, the program will show the error message box for the user to configure the material. During the configuration process, the GUI will feedback to the user with error alert message boxes if each conditional statement is not satisfied, so that the user can follow the flowchart below.

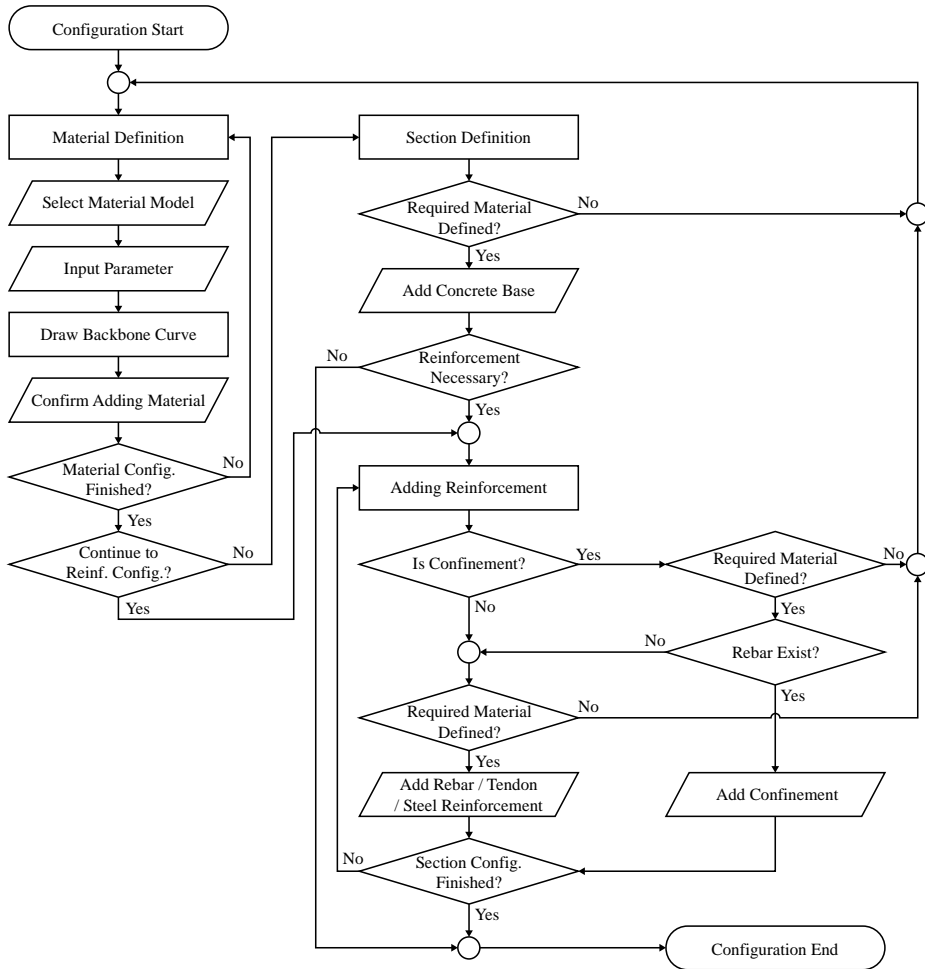


Figure 4-5 Total configuration process of the developed program

As the section information is set, the main view of the program shows the cross-sectional diagram where the user can arrange all kinds of reinforcements easily and visually.

In addition, the program can carry multiple sections in a project file so that the user can compare several element designs at once.

After following the process shown in **Figure 4-5**, the program can analyze the sections provided by the user.

4.4 Performing Analysis

4.4.1 General analysis process

The developed program analyzes reinforced concrete sections and gives two kinds of results: moment-curvature interaction and P-M interaction. When the program starts analyzing, it uses the given sections' information, analysis options, and interaction calculations.

The Analyzer has two major solvers for the moment-curvature interaction and P-M interaction. In essence, the solvers' calculation process is based on trial and error. When the error of each step goes under 10^{-6} unit, then the step will be stopped and the next calculation performed.

These processes are shown in **Figure 4-6** to **Figure 4-8**. **Figure 4-6** is the main flow of the Analyzer class that calls the functions shown in **Figure 4-7** and **Figure 4-8**.

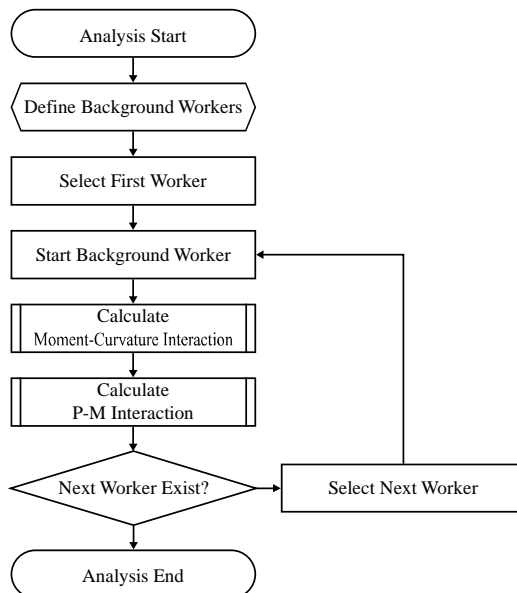


Figure 4-6 Main routine of Analyzer class

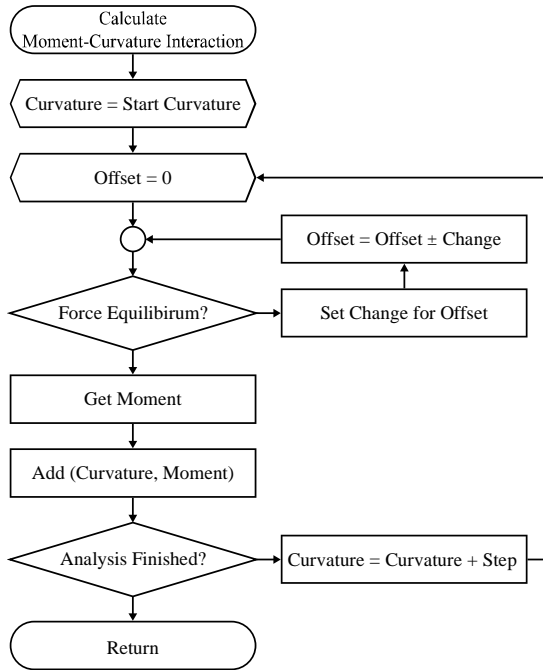


Figure 4-7 Function for obtaining the moment-curvature interaction.

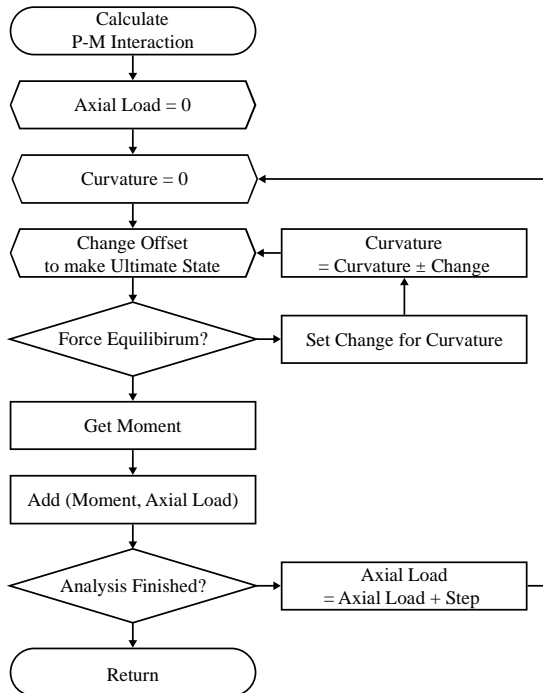


Figure 4-8 Function for obtaining the P-M interaction.

The Analyzer performs all calculations with background workers allocated by the section configuration where one worker processes one section.

The analysis options provide some information necessary for analysis and provide the maximum micro-section size, curvature increment, and curvature range. The details for each option are explained in **Table 4-2**.

Table 4-2 Details of analysis options.

Category	Options	Role
Accuracy & Speed ^a	Maximum Micro-Section Size	The Analyzer divides a section into many micro-sections; the height and width of micro-sections are less than this variable.
	Curvature Increment	This variable is used as the step increment of curvature while calculating the moment-curvature interaction.
	Axial Load Increment	This variable is used as the step increment of axial load while calculating P-M interaction.
Curvature Range	Minimum Curvature	The Analyzer calculates the minimum curvature to maximum curvature. This option is useful when the user wants to know the residual moment after the ultimate state.
	Maximum Curvature	

a. The variables in this category are smaller so that the analysis result will be more accurate. If they are larger, then the result will be less accurate, but the user can obtain results faster.

The user can determine the accuracy or speed of the analysis by controlling the analysis options. For example, the user should set the **Curvature Increment** option small enough to obtain an accurate cracking moment. If not, the exact points (cracking moment, yielding moment, ultimate moment) cannot be determined accurately although the analysis speed is faster.

4.4.2 Prestressed elements with unbonded tendons

Unlike other structural components, unbonded tendon components do not satisfy the strain compatibility assumption mentioned in **Section 2.2.3**. The prestressed element with unbonded tendons is analyzed differently in the developed program. Furthermore, the relationship between tendon stress variation and normalized load, derived as **Eq. (3-3)**, is used in the analysis.

The user must input the stress increase, Δf_{ps} , when configuring the setting. The Analyzer checks whether the unbonded tendon exists or not, and carries out appropriate processes. **Figure 4-9** shows the tendon configuration window showing how the tendon is configured.

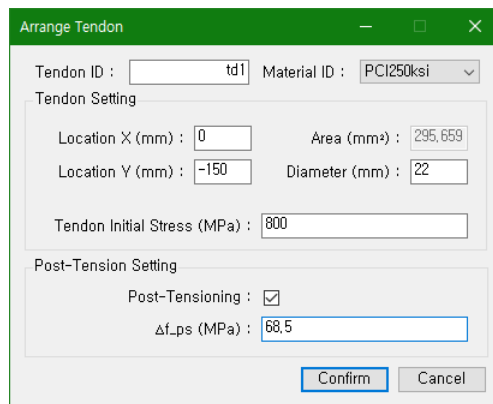


Figure 4-9 Tendon configuration

The entire analysis process follows the diagram in **Figure 4-10** to **Figure 4-12** containing a multi-fold iteration structure that can elongate the computing time. By optimizing the sub-routine and using multithreaded computing, the time is minimized as much as possible.

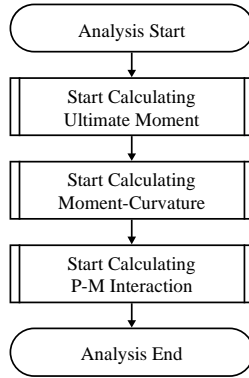


Figure 4-10 Main routine of Analyzer class with unbonded tendons

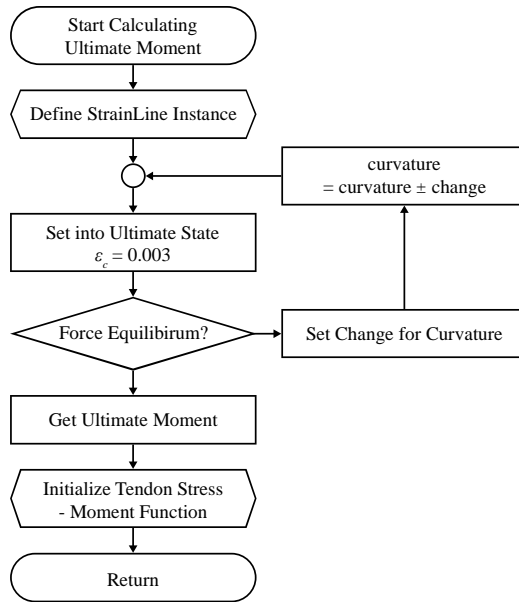


Figure 4-11 Sub-routine for calculating ultimate moment with unbonded tendons

The main routine of the Analyzer class with unbonded tendons is changed. Unlike normal reinforced concrete or prestressed concrete with bonded tendons, the ultimate moment must be calculated first. The ultimate moment value is used in the step described hereafter.

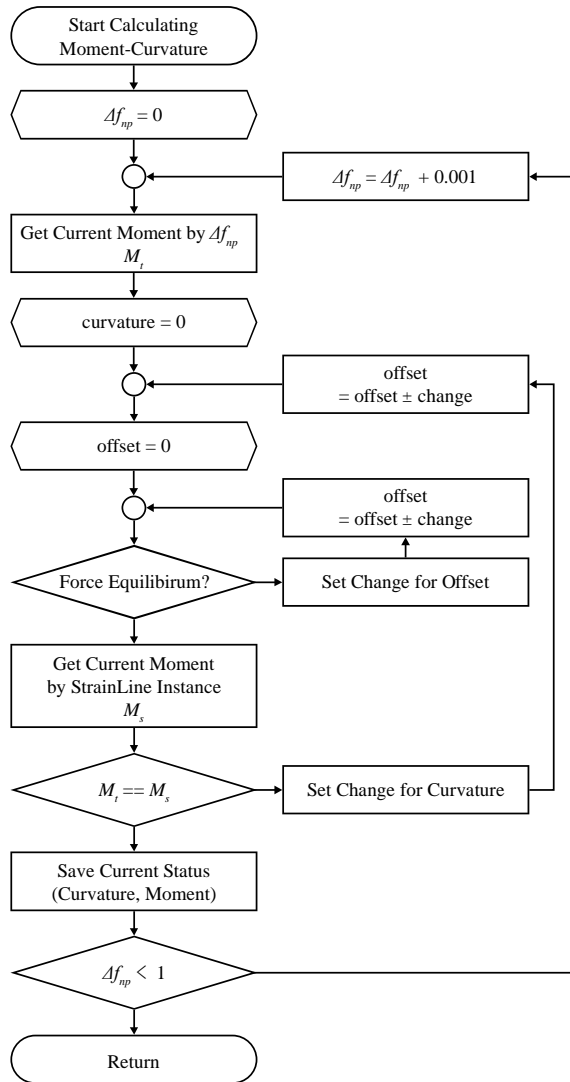


Figure 4-12 Sub-routine for calculating moment-curvature relationship with unbonded tendons

As shown in **Figure 4-12**, the normalized tendon stress increase, Δf_{np} , is initialized at first. Usually the moment is calculated based on curvature, but in this process both curvature and moment are determined by normalized tendon stress.

The Analyzer receives the current normalized moment determined by tendon increase, M_t , using Δf_{np} . The equation for normalized tendon stress increase and normalized load, **Eq. (3-3)**, is used in this step. The following equation can be determined from **Eq. (3-3)**.

$$\Delta f_{np} = M_t e^{4.13(M_t - 1)} \quad (4-1)$$

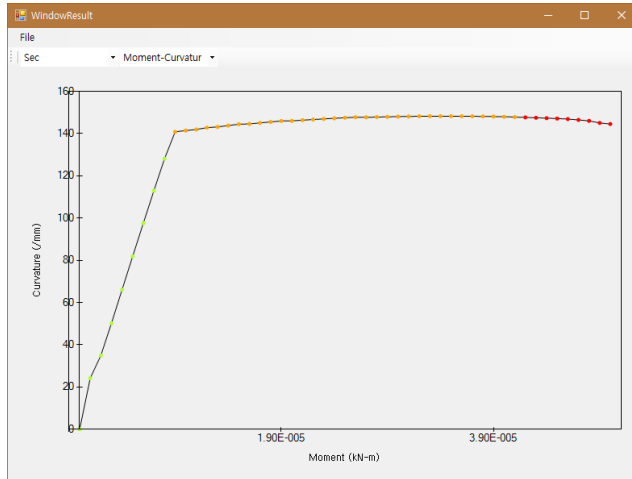
Since Δf_{np} is already determined, M_t value is necessary. Equation (4-1) should be converted into the reverse equation to be used for analysis. Lambert (1758) considered the solution known as Lambert's transcendental equation. Then, Euler (1783) used the equation for solving the special case (like **Eq. (3-3)**) and provided an early version of Lambert W function. Using Lambert W function, **Eq. (4-1)** can be converted into the reverse equation as:

$$M_t = \frac{1}{4.13} W(4.13 e^{4.13 \Delta f_{np}}) \quad (4-2)$$

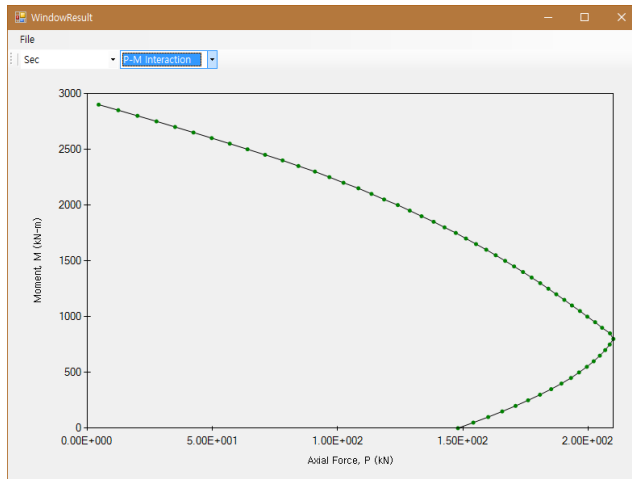
Consequently, the Analyzer initializes the StrainLine instance and makes both curvature and offset zero. By changing them a little bit and continuously undergoing trial and error, the program will find appropriate curvature and moment. There are two kinds of moment values in the process: one calculated from **Eq. (4-2)** and one calculated from section information by StrainLine instance. The continuing trial and error is carried out based on comparing these two moments. If they are the same, then the program will save the current status to the ResultData instance. If not, StrainLine instance will be changed. The program will rematch these two moments continuously until they are same. Whenever each step is finished, Δf_{np} increases and the program will restart the whole trial and error process for the next step. The calculation will be finished when the tendon stress reaches the ultimate state.

4.5 Example of Results of Analysis

Once the entire process is completed, the ProjectManager class takes and saves the result data as shown in the new window dialog with a chart. Using combo boxes, the user can read the moment-curvature interaction and P-M interaction chart as shown in **Figure 4-13**.



(a) Moment-curvature interaction diagram



(b) P-M interaction diagram

Figure 4-13 Charts in the result dialog

The chart gives some information with colored dots in green, yellow, and red which refer to the elastic state, the post-yield state, and the post-ultimate state, respectively. The user can read some sketchy information from the chart view.

If the user wants to take the exact figure data, not a chart, then the figure data can be obtained by exporting to a CSV(Comma-Separated Values) file. Spreadsheet programs (e.g. Microsoft Excel) can read this file and the user can process it for the study.

4.6 Summary

In this chapter, the structure, algorithm, and features of the developed program are reviewed. The following is a summary of this chapter:

1. C# is used as the programming language for systematic development and easy expansion of the program. GUI (Graphical User Interface) helps users to use the program intuitively.
2. Program structures are well-organized, allowing for adding new features easily, including new material model, shape, and analytic method, etc. Hierarchical interfaces and classes make the program work well.
3. The interactive interface and configuration process of materials, sections, and components is designed for users to analyze and design the sections from normal RC elements to unbonded prestressed concrete elements.
4. Analysis process is designed in separate ways for general elements and unbonded prestressed elements. The general elements include normal RC elements and bonded prestressed elements, which satisfy the force equilibrium and the strain compatibility. Unbonded prestressed concrete elements do not follow the strain compatibility. The tendon behavior of unbonded prestressed elements is described using a new relation between the tendon stress increase and moment, aforementioned in the previous chapter.
5. Results of analysis are provided in the chart window with different color dots which refer to various element states. The data can be exported as a CSV file that can be opened in spreadsheet programs.

Chapter 5. Analysis Results and Verification

In the previous chapters, it was described that a new program is developed with appropriate algorithms and the new interaction formula is assigned well. In this chapter, verification of the new program is performed.

There are various types of sections: unconfined concrete section, confined concrete section, bonded/unbonded prestressed concrete section, and so on. Each one can be subdivided into several sections; unconfined sections, for example, include steel reinforced concrete (SRC) section, doubly reinforced concrete section, and so on. Among several examples of section, some can be calculated easily by hand. In the hand calculation, however, the nominal moment is calculated usually with Whitney rectangular stress block (Whitney, 1937).

Given that the Whitney rectangular stress block was developed with approximate values for easy calculation, hand calculation is not appropriate for the verification of the developed program. Instead of hand calculation, BIAX (Wallace, 1992) is used for verification.

The BIAX is a well-verified computer program to calculate moment-curvature relation and P-M interaction. This program was developed for use on MS-DOS originally, but modified again for use on legacy Windows (e.g. Windows 95, 98 and XP) in 1996. For now, this program is totally incompatible on modern Windows (e.g. Windows 7, 8, and 10), since windows had given up the MS-DOS compatibility. Thus, through using virtual machine that Windows XP is installed (**Figure 5-1**), the verification comparing between BIAX and the newly developed program in this study is carried out.

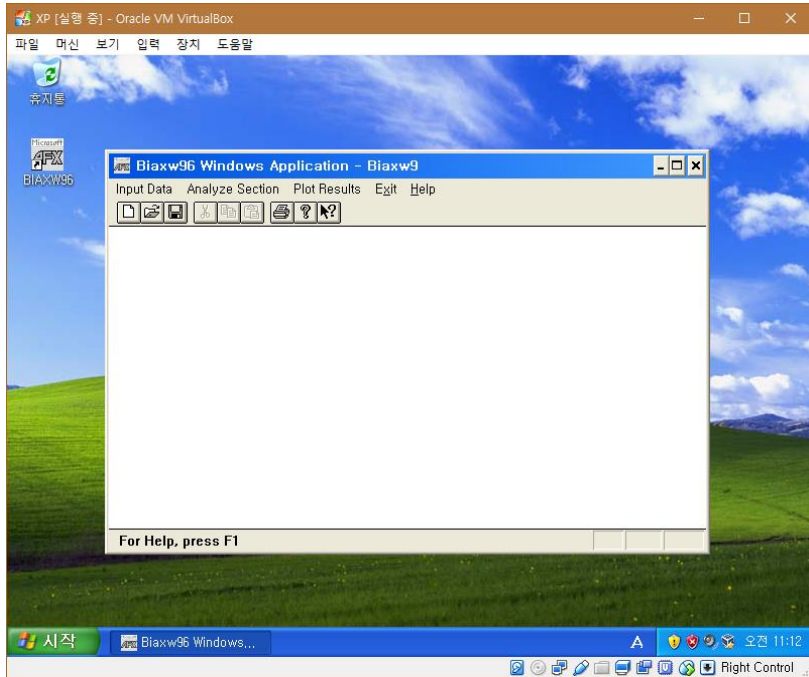


Figure 5-1 Virtual machine environment for using BIAX

During using the BIAX, although all analysis is performed well, BIAX shows error messages when the resultant diagrams are shown. This problem usually occurs when the resultant data has over hundreds of points. In addition, BIAX does not have a feature for exporting the exact coordinates of the moment-curvature diagram and P-M interaction as any type of files. Due to these problems, the diagrams shown in the following sections are drawn using the extracted data from the result file directly, whose file extension is “DAT”.

Meanwhile, BIAX does not support the bonded prestressed section. Verification of the developed program for bonded prestressed section is carried out through comparing with the term project results from the Post-tensioned Concrete Structures class held at the University of Illinois at Urbana-Champaign (Kang, 2016). Three submissions are used to compare with the new developed program in this study.

In addition, some cases are not possible to be calculated by hand and even

other programs. For example, unbonded prestressed section cannot be calculated by either hand or other computer programs to the author's knowledge. Unbonded prestressed section does not follow the assumptions from ACI 318 Design Code as previously mentioned. Several finite element programs have features for modeling unbonded prestressed elements, but no programs can generate moment-curvature relations of unbonded prestressed concrete sections. Comparison with existing experimental data may be the only way for indirect verification.

5.1 Verification Using Cases with Various Conditions

The sections for verification vary from conventional RC section to unbonded post-tensioned section, depending on which components are used in the sections. In this chapter, the verifications of the followings are performed: unconfined RC sections, confined RC sections, and bonded prestressed concrete section.

5.1.1 Unconfined reinforced concrete section

As the unconfined reinforced concrete section for verification, the sample is selected as **Figure 5-2**. This sample refers to the Example 1 from the BIAX: Revision 1 (Wallace, 1992), which is the manual for BIAX.

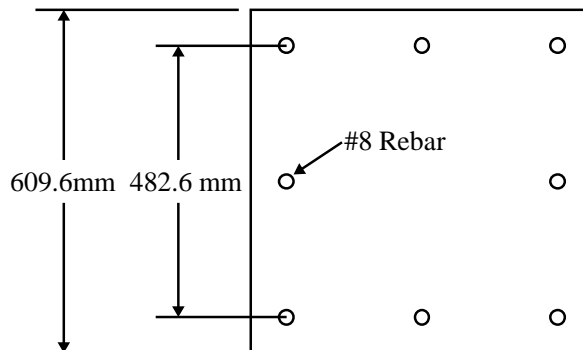


Figure 5-2 Sample 1: Cross section of unconfined concrete section

The sample has the square cross section shape, whose width and height are 609.6 mm. There are 8-#8 rebars in the section with 50.4 mm of clear cover at concrete sections. The concrete material follows the modified Kent and Park model with 3.4 ksi (23.44 MPa) strength (shown in **Figure 5-3**) and the rebar material follows the bilinear steel model with 60 ksi (413.7 MPa) yield strength (shown in **Figure 5-4**).

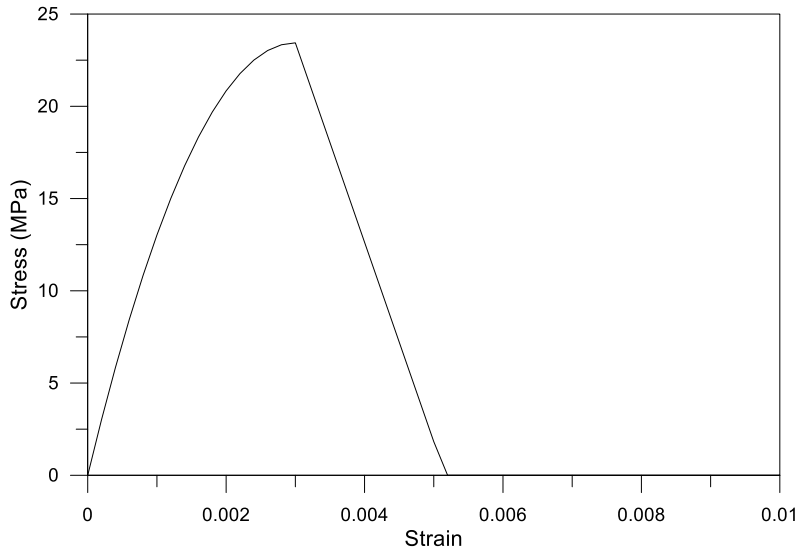


Figure 5-3 Sample 1: Concrete material model

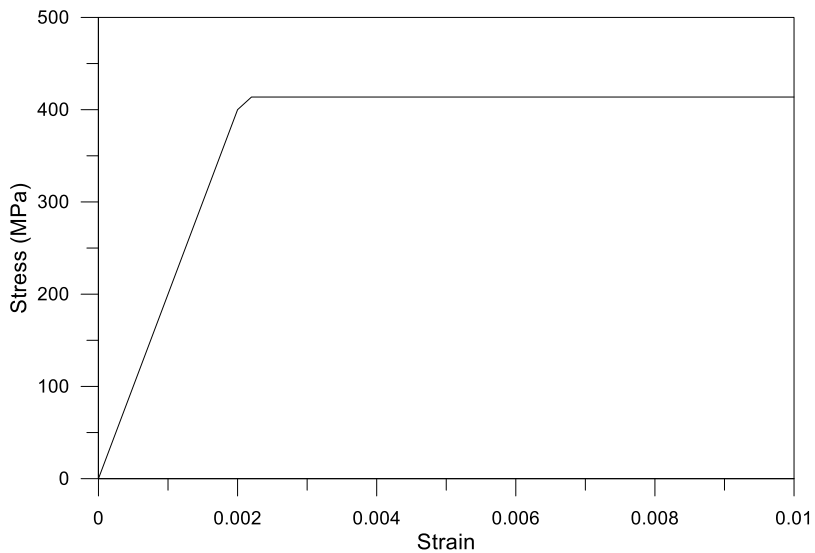


Figure 5-4 Sample 1: Steel material model

The setting that reinforced concrete area is divided into 12 by 12 cells is assigned equally at the developed program as shown in **Figure 5-5**. In the each step size of curvature and axial force is not same, but by making the step size small enough, the result data can be compared to each other well.

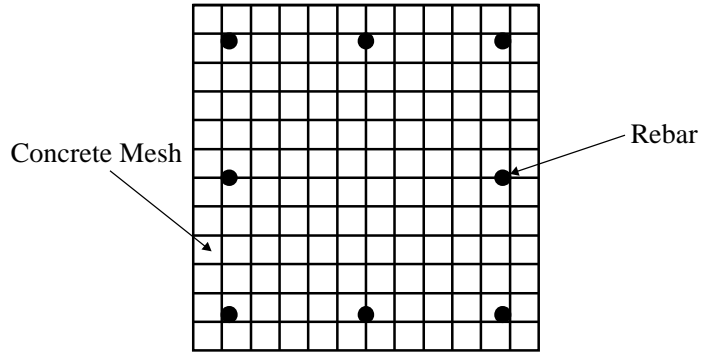


Figure 5-5 Sample 1: Mesh generation

With the conditions mentioned above, the moment-curvature diagram and P-M interaction data derived from the both programs are shown in **Figure 5-6** to **Figure 5-7**.

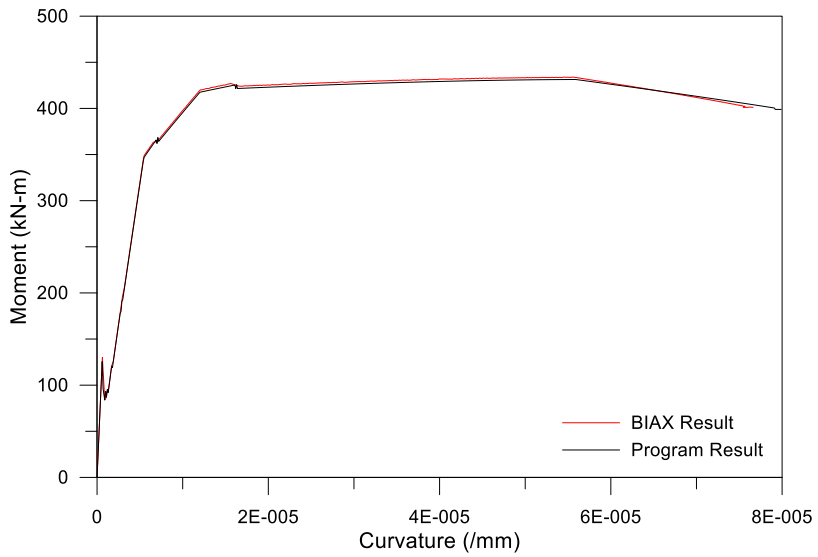


Figure 5-6 Sample 1: Moment-curvature comparison

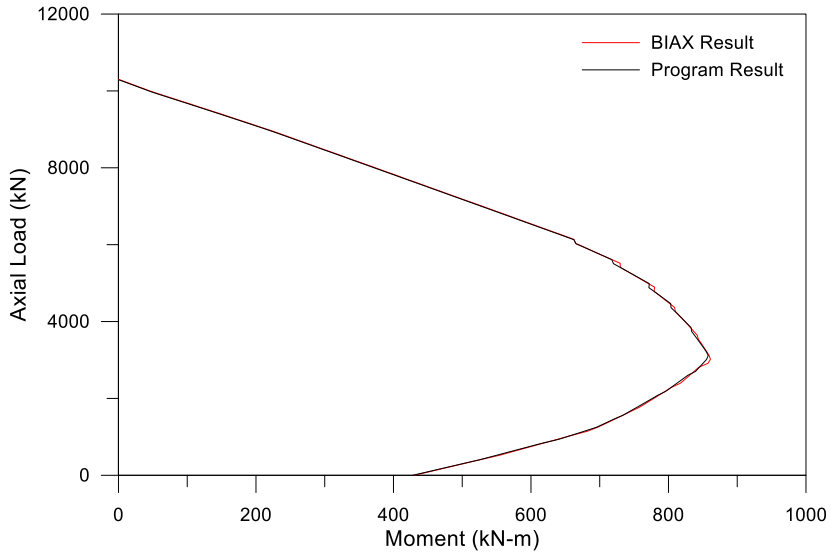


Figure 5-7 Sample 1: P-M interaction comparison

Overall, two analysis results show almost the same. The difference rate between BIAx and the developed program is under 0.5% at the ultimate state. The cracking moment and yielding moment shows almost same as well.

5.1.2 Confined reinforced concrete section

As the unconfined reinforced concrete section for verification, the sample is selected as **Figure 5-8**. This sample refers to the example 2 from the BIAX: Revision 1 (Wallace, 1992).

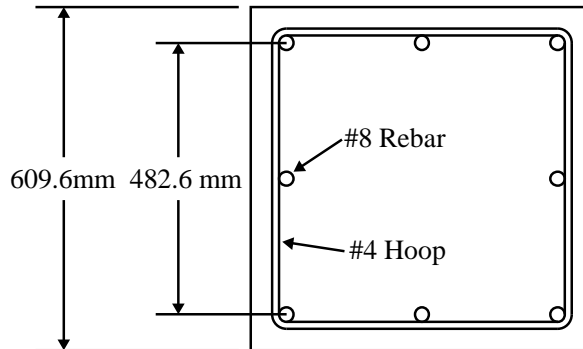


Figure 5-8 Sample 2: Cross section of confined concrete section

The sample has totally same condition with the sample of **Section 5.1.1**, except including a #4 square hoop around the rebars. The both of unconfined and confined concrete materials follow the modified Kent and Park model as shown in **Figure 5-9**.

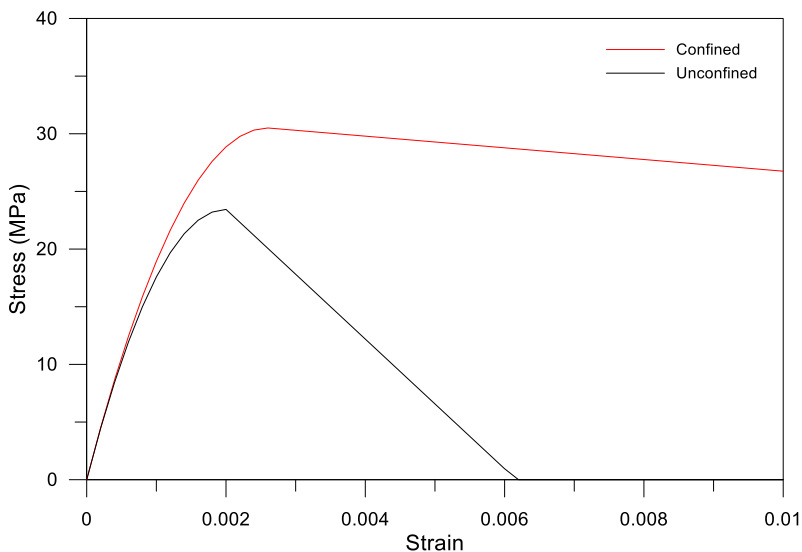


Figure 5-9 Sample 2: Unconfined and confined concrete models

The concrete model has same strength (3.4 ksi), but the parameters for the models are different from the sample of **Section 5.1.1** (e.g. the strain at the maximum strength). In the case of steel, the same model provided in **Section 5.1.1** is used for this sample.

BIAX set the confined area inconveniently through choosing the mesh number. However, in the new developed program, user can just add the transverse reinforcement through choosing four-corner rebars and the confinement area will be set automatically. The user interface is different, but generated mesh information is totally same in this sample.

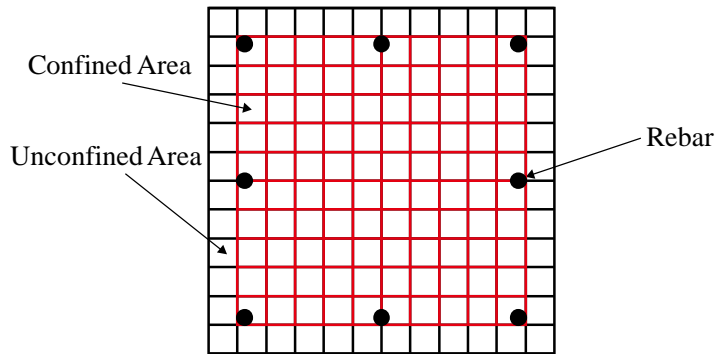


Figure 5-10 Sample 2: Mesh generation

With the conditions mentioned above, the moment-curvature diagram and P-M interaction data derived from the both programs are shown in **Figure 5-11** to **Figure 5-12**.

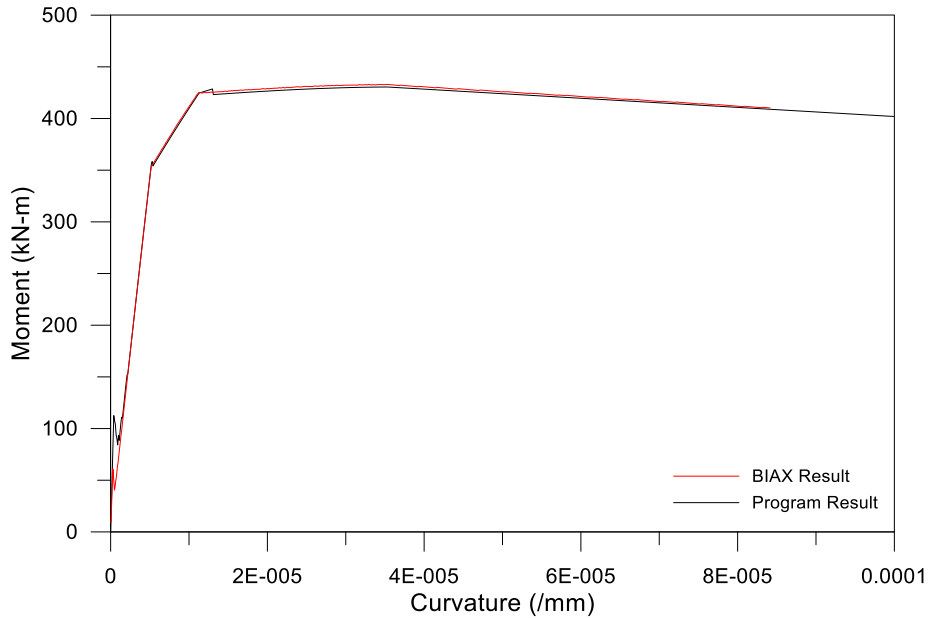


Figure 5-11 Sample 2: Moment-curvature comparison

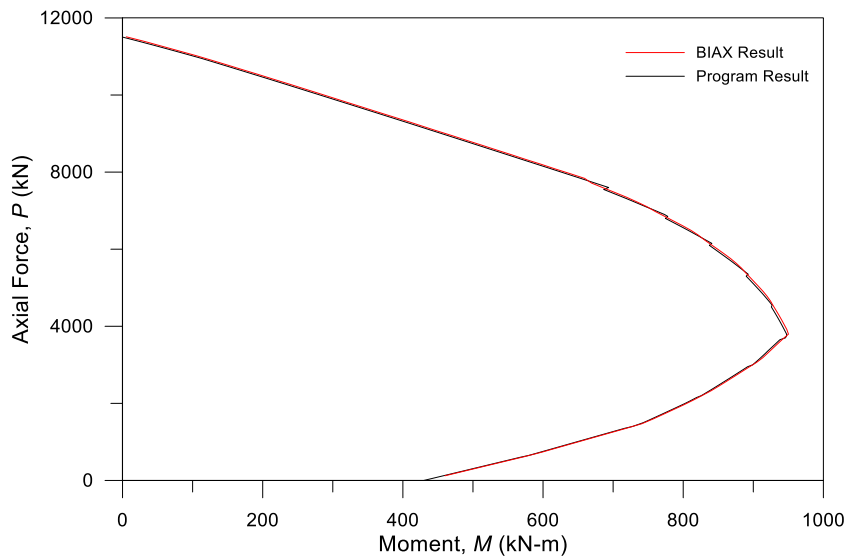


Figure 5-12 Sample 2: P-M interaction comparison

Overall, two analysis results show almost the same. The difference rate between BIAX and the developed program is under 0.5% at the ultimate state in this case as well.

5.1.3 Bonded prestressed concrete section

The sample of bonded prestressed concrete section is extracted from Post-tensioned Concrete Structures class (Kang, 2016), as shown in **Figure 5-13**.

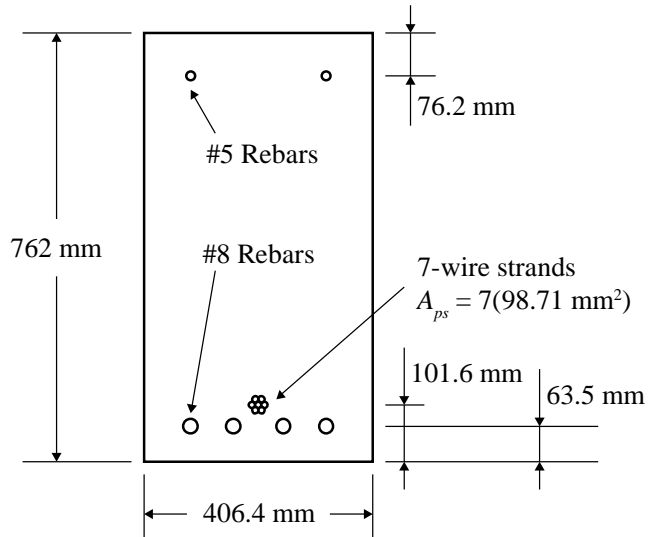


Figure 5-13 Sample 3: Cross section of bonded prestressed concrete section

The sample has the dimension of 406.4 mm by 762 mm. There are 2-#5 top rebars and 4-#8 bottom rebars. Seven-wire strands are selected as a bonded tendon in this section. The concrete model follows the Hognestad model, with 27.6 MPa (4 ksi) maximum strength at 0.002 strain as shown in **Figure 5-14**.

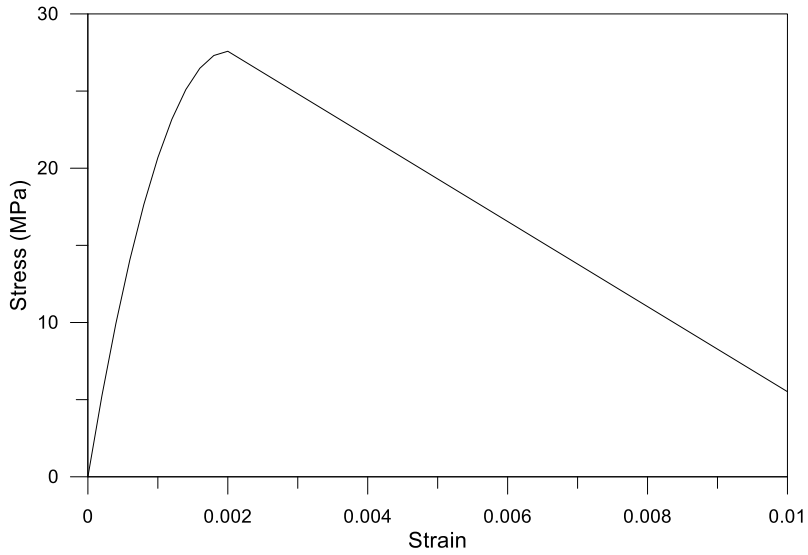


Figure 5-14 Sample 3: Concrete model

The rebar model follows the bilinear steel model (same with the model of **Section 5.1.1**), and the tendon model follows the PCI tendon model with 270 ksi (approx. 1860 MPa) as shown in **Figure 5-15**.

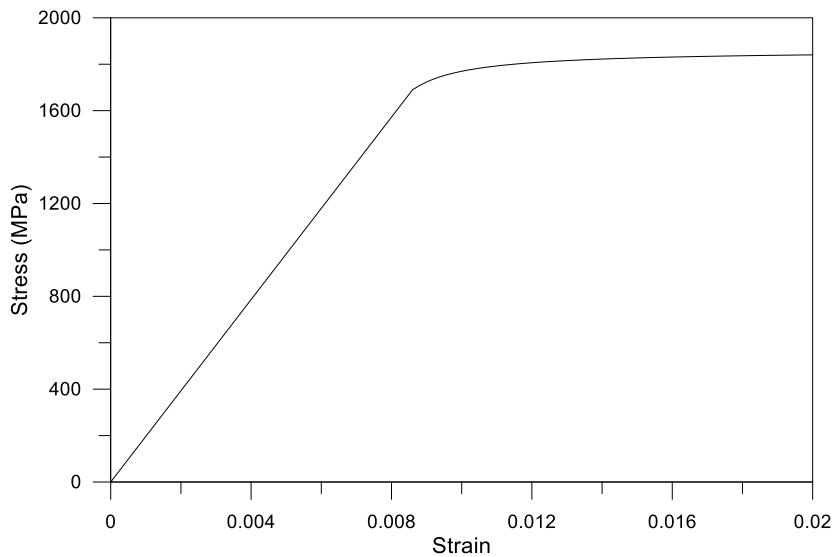


Figure 5-15 Sample 3: Tendon model

With the conditions mentioned above, the moment-curvature diagram derived from the programs is shown in **Figure 5-16**. The comparison is carried out with the other students' assignment submissions from Post-Tensioned Concrete Structures class (Kang, 2016).

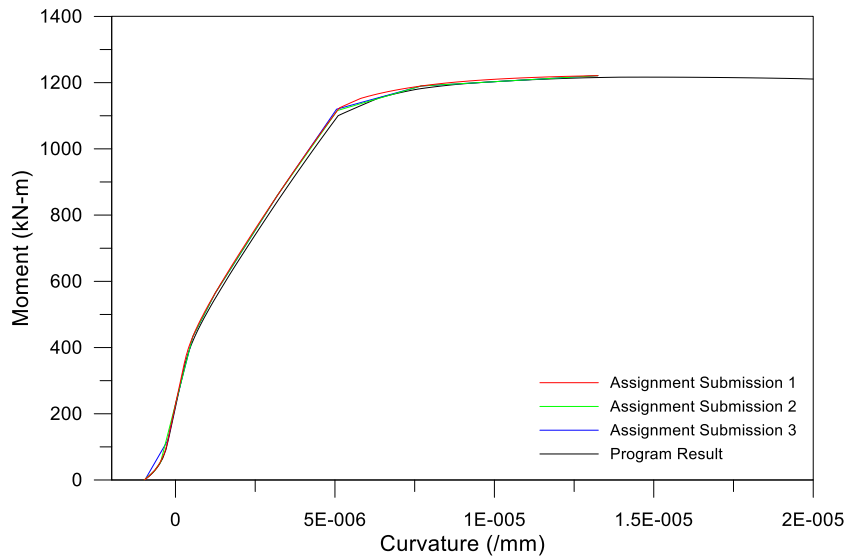


Figure 5-16 Sample 3: Moment-curvature comparison

Overall, four analysis results show almost the same. The differences are occurred because of the degree of calculation accuracy. Submissions used their own spreadsheets and Matlab codes for calculation, and mesh generations are different as well. However, all results by various algorithms and meshes show same tendencies.

5.2 Discussion

In the previous section, only reinforced and bonded prestressed concrete sections are compared with the pre-existing data or software. The comparison shows good similarity between the new and previous analysis data.

In **Section 3.2**, the relation between tendon stress increase and moment is developed for model sensitivity studies on unbonded prestressed concrete sections. This is conducted because no pre-existing sectional analysis data are available for unbonded sections. The model is developed to represent limited cases of the relations. The model may not cover the whole experimental cases. For example, the specimen A-6 and A-9 from Tao and Du (1985) shows almost linear tendency, as shown in **Figure 3-5**. Given the issue, an in-depth case study is necessary for reasonable explanation.

In this section, case studies of unbonded prestressed elements with several types of the relations between tendon stress increase and moment. The exponential stress increase model is already defined as **Eq. (5-1)**. Additionally, linear (**Eq. (5-2)**) and bilinear (**Eq. (5-3)** and **(5-4)**) relations are defined as follows:

$$\Delta f_{np}^f = M_t e^{4.13(M_t - 1)} \quad (5-1)$$

$$\Delta f_{np}^f = M_t \quad (5-2)$$

$$\Delta f_{np}^f = 0.05M_t \left(\text{when } x < \frac{19}{19.95} \right) \quad (5-3)$$

$$\Delta f_{np}^f = 20M_t \left(\text{when } x \geq \frac{19}{19.95} \right) \quad (5-4)$$

The stress increase models used in this section are shown in **Figure 5-17**. Given the previous studies mentioned in **Section 0**, the bilinear tendon stress

increase model is exaggerated model simulating sudden bond breakage, but it will show the sensitivity of the difference of models on the moment-curvature relation well.

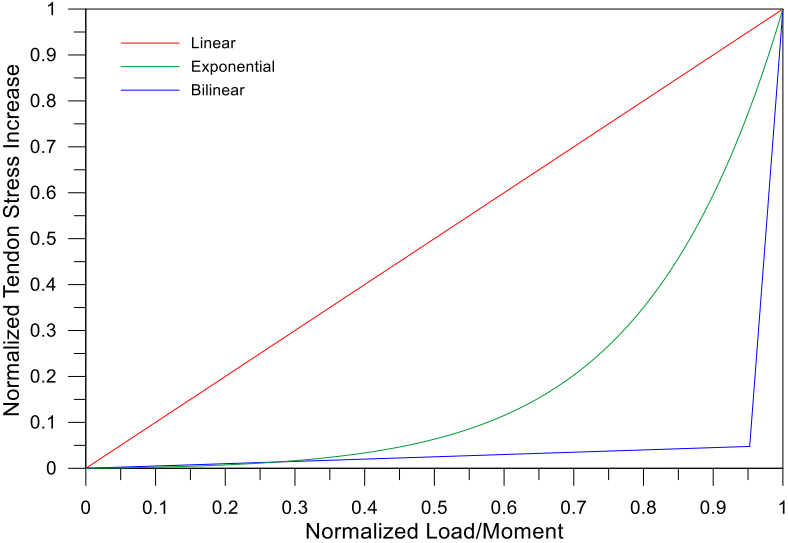


Figure 5-17 Tendon stress increase models

5.2.1 Case study 1

The sample of unbonded prestressed concrete section is extracted from Post-Tensioned Concrete Structures class taught by Prof. Kang at the University of Illinois at Urbana-Champaign (2016), which is the same example (Sample 3) in **Section 5.1.3**. Only the bonded condition is different. The cross-section is shown in **Figure 5-18**.

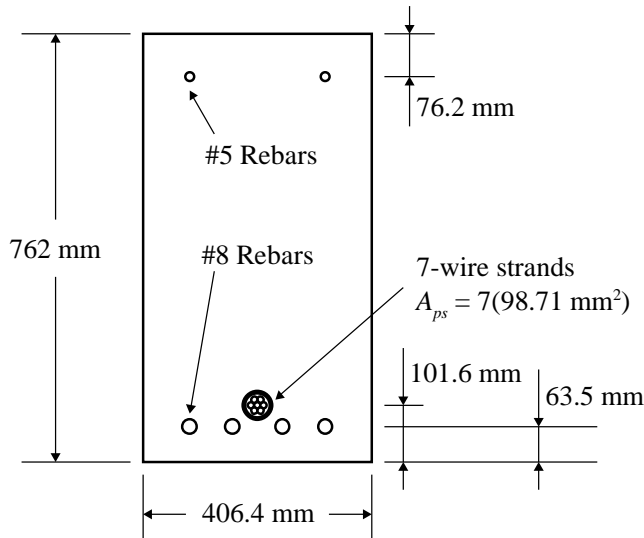


Figure 5-18 Case study 1: Cross section of unbonded prestressed concrete section

The tendon is unbonded for Case study 1. The ultimate stress of the tendon, f_{ps} , is set as 1310.4 MPa, which is calculated using the f_{ps} model by Naaman et al. (2002). The Mattock (1979) model is used for the tendon stress-strain model. The linear, bilinear, and exponential tendon stress increase models shown in **Figure 5-17** are used for the study, and compared with each other. The unbonded prestressed concrete sectional analysis results depending on the several tendon stress increase models are shown in **Figure 5-19**.

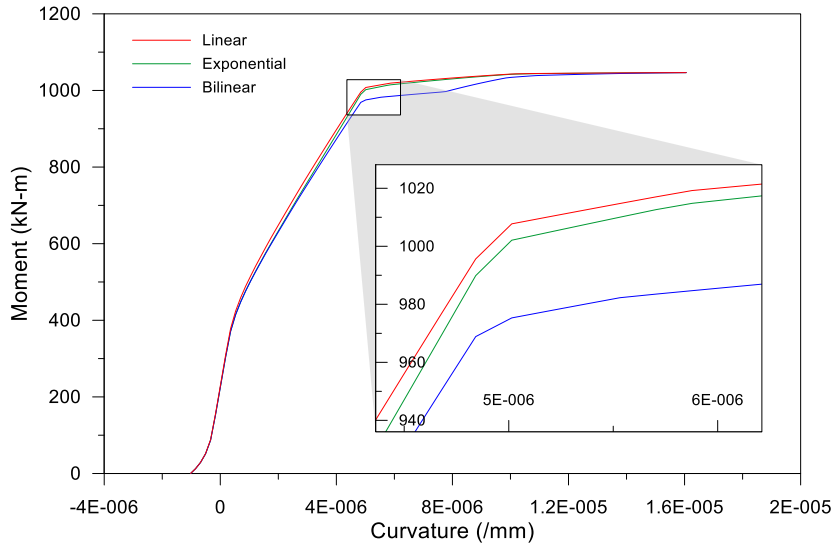


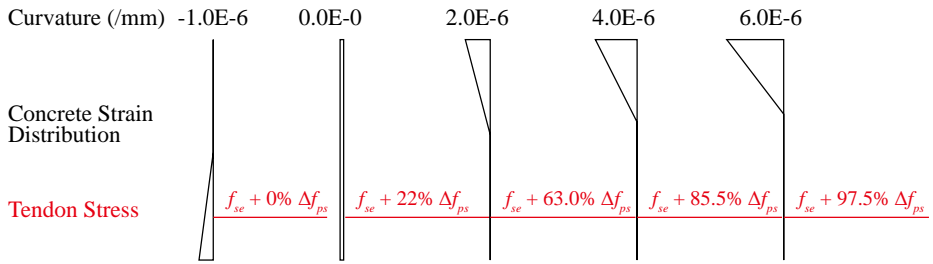
Figure 5-19 Case study 1: Moment-curvature relations

The analysis of linear and exponential models shows almost the same results, although the result with the exponential model shows smaller moment values in general nonlinear range.

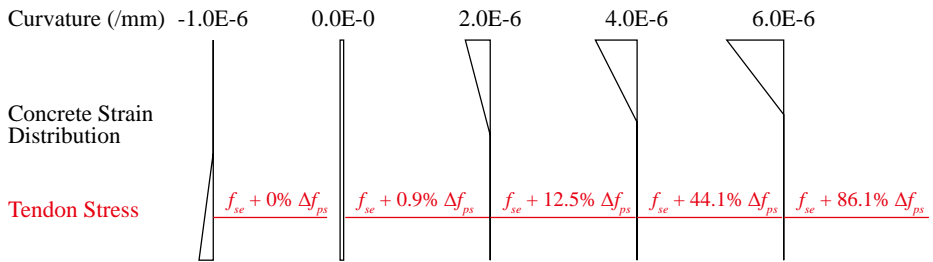
The result with the bilinear tendon stress increase model shows a different tendency, compared with the others. The yield moment is around 40 kN-m less than the others. In addition, the tendency is different in the range from the yield point and ultimate point. It shows a sudden increase of moment even after the yield point. Even so, the largest difference of moment is still under 4% of the ultimate moment.

The tendon increase rate of each model at each curvature is shown in **Figure 5-20**. All models show different tendon increases at the same given curvature. The tendon increase rate at each curvature is quite different with each other. However, the resulting internal moments at each curvature is not so much different.

Case study 1: Linear tendon stress increase



Case study 1: Exponential tendon stress increase



Case study 1: Bilinear tendon stress increase

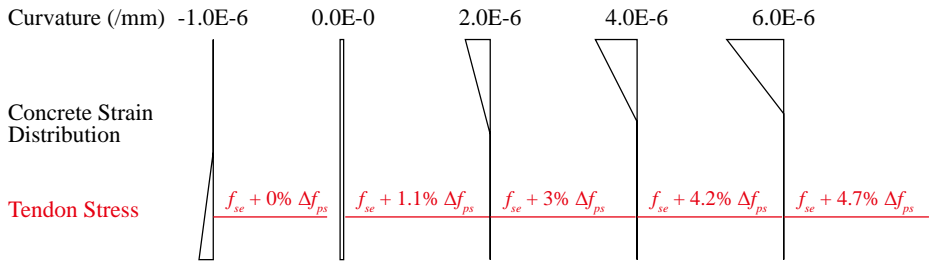
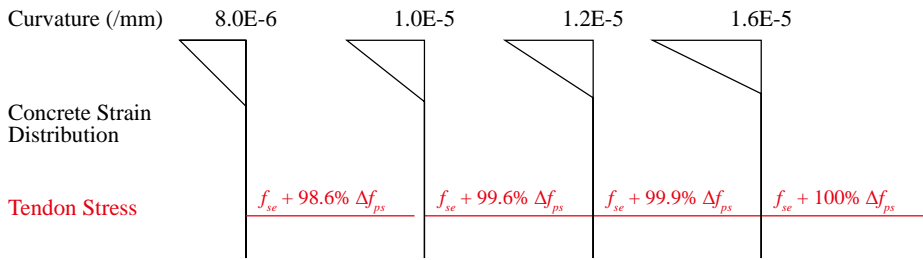
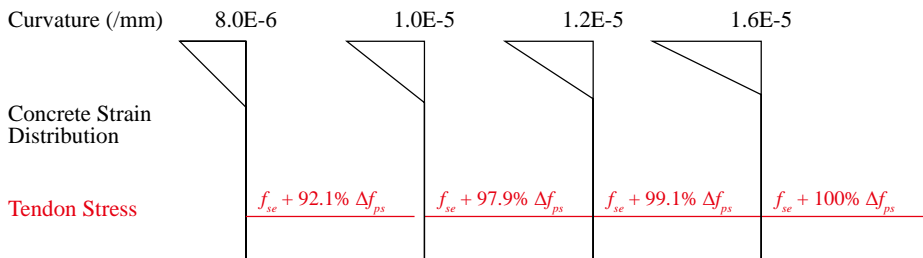


Figure 5-20 Case study 1: Tendon increase rate at each curvature (continued)

Case study 1: Linear tendon stress increase



Case study 1: Exponential tendon stress increase



Case study 1: Bilinear tendon stress increase

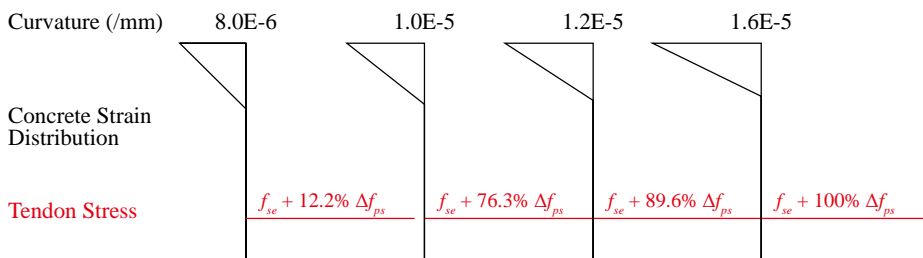


Figure 5-20 Case study 1: Tendon increase rate at each curvature

5.2.2 Case study 2

For looking into the effect of the tendon stress increase models, the sectional element having only tendons without any mild steel bonded reinforcements is analyzed. The cross-section is shown in **Figure 5-21**.

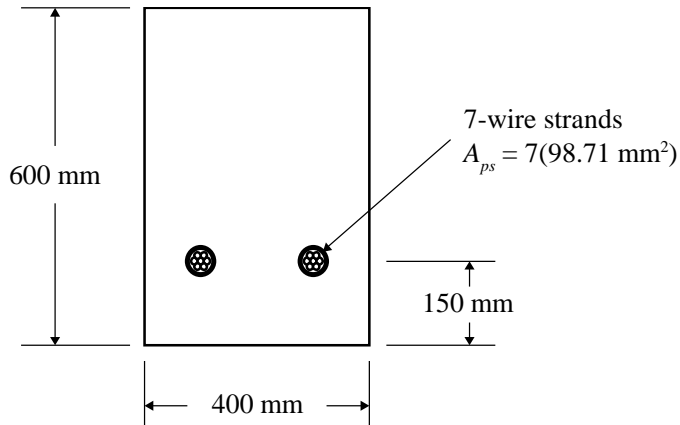


Figure 5-21 Case study 2: Cross section of unbonded prestressed concrete section

The ultimate stress of the tendon, f_{ps} , is set as 1310.4 MPa, which is calculated using the model by Naaman et al. (2002). The Mattock (1979) model is used for the unbonded tendon stress-strain model. Like **Section 5.2.1**, the linear, bilinear and exponential models are used. The analysis results are shown in **Figure 5-22**.

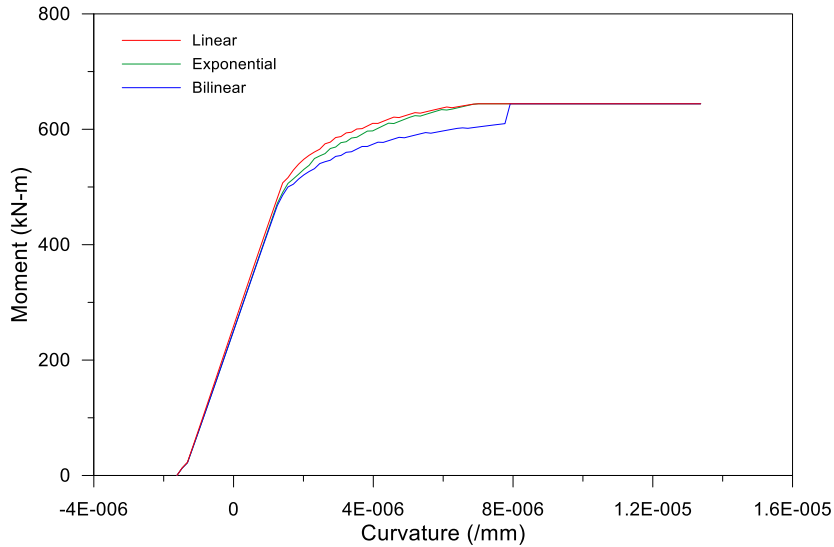


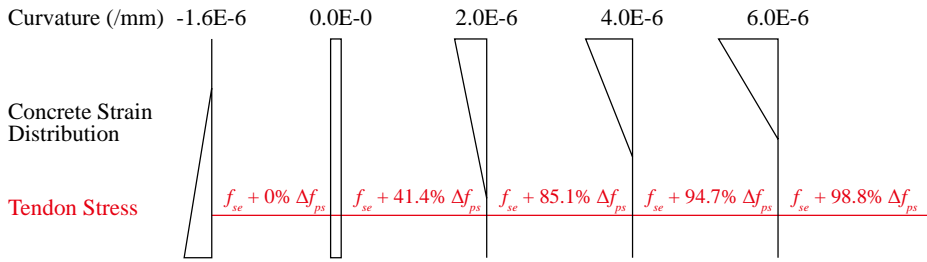
Figure 5-22 Case Study 2: Moment-curvature relations

As assumed, the unbonded prestressed element without any rebars shows the difference among the models better than the first case study. The analysis using the linear and exponential models shows similar results, but the difference rate is larger than the first case study.

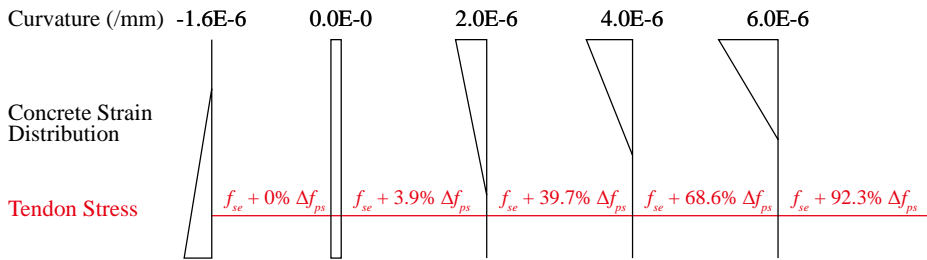
The tendency when the bilinear model is used is quite different totally. It shows a sudden increase of moment before reaching the ultimate moment similar to the first case study, but the increase rate is much higher. The largest difference of moment values among the tendon stress increase models is still around 6% of the ultimate moment; this is a bit larger than the first.

The tendon increase rate of each model at each curvature level is shown in **Figure 5-23**. All models show different tendon increases at the same curvature.

Case study 2: Linear tendon stress increase



Case study 2: Exponential tendon stress increase



Case study 2: Bilinear tendon stress increase

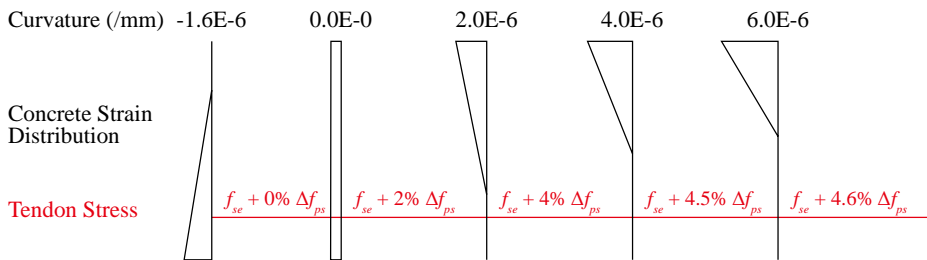
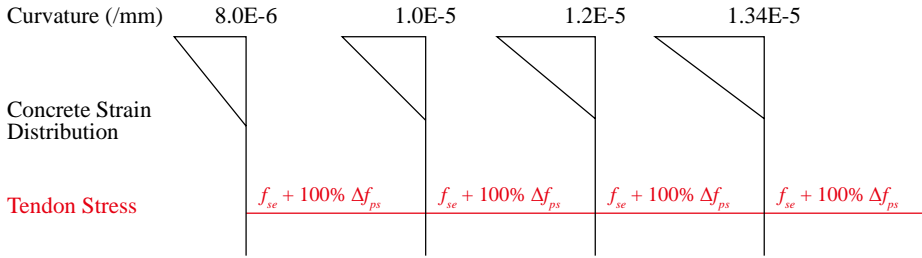
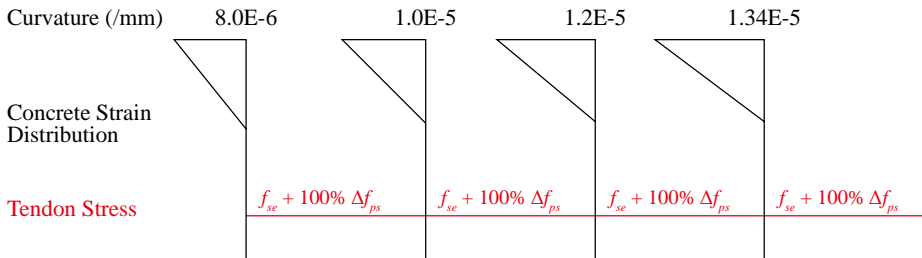


Figure 5-23 Case study 2: Tendon increase rate at each curvature (continued)

Case study 2: Linear tendon stress increase



Case study 2: Exponential tendon stress increase



Case study 2: Bilinear tendon stress increase

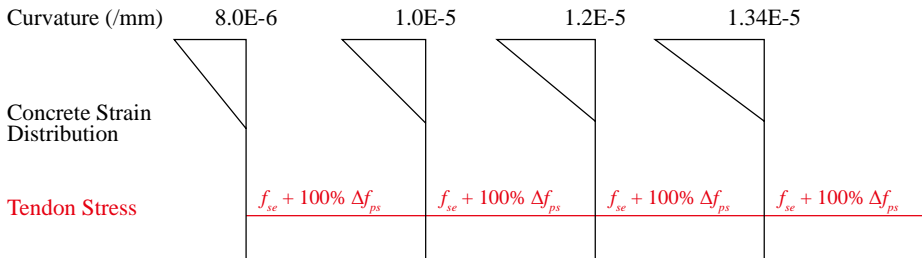


Figure 5-23 Case study 2: Tendon increase rate at each strain

Unlike the first case study, the unbonded prestressed element without any rebars shows the maintained moment value and tendon stress over the large range of nonlinear deformations. Tendon stresses of the models at each curvature are substantially different, but the strain distribution is almost the same.

5.2.3 Summary

Both case studies in this chapter show that the effect of the selected tendon stress increase model is relatively small. In **Section 3.2**, the tendon stress increase model is developed through curve fitting. There has been no extreme experimental bilinear relation like the model used in the case studies. Most test results showed the exponential increase, and only some previous test specimens showed the linear-close increase. As shown in **Figure 5-19**, there are only minor differences in regard to moment-curvature relationship between the linear and exponential models.

The bilinear model is an abnormally-emphasized model as aforementioned; thus, it may be unnecessary to consider in depth. However, the bilinear model provides a good information regarding the moment difference between the elements with effective tendon stress and nominal tendon stress.

Despite of the moderate effect of tendon stress increase, the proper tendon stress increase model is necessary to generate reasonable moment-curvature relations. Therefore, the bilinear tendon stress model is not recommended, but either the linear and exponential model is recommended.

Chapter 6. Conclusion

In this study, a new sectional analysis program is developed that can be used as a platform for the design and analysis of reinforced and prestressed concrete structures. The newly developed program shows good analysis results comparing with the pervious well-verified program, BIAX, and previous efforts.

This study focuses on the fusion research of computer programming and structural engineering. The program does not support only conventional RC section with normal concrete and mild steel, but also unbonded and bonded prestressed concrete section with post-tensioning tendons, as well as the section with high-strength materials. For example, the P-M interaction of PT segmental bridges and PT walls can be analyzed by this program. The backbone curve of plastic hinges with and without axial force can be calculated as well. Through the development of the platform for sectional analysis, future researchers and engineers are expected to save their time.

The sectional analysis including the calculation of moment-curvature relation and P-M interaction have been previously researched, and the previous studies and programs have supported only up to bonded prestressed concrete elements. In the case of unbonded prestressed elements, the complex physical issues (e.g. tendon friction in the sheathing) makes the sectional calculation tough. Therefore, a new analytic model for the relation between the unbonded tendon stress increase and the load or moment is established. Additionally, very high-strength and/or lightweight concrete models are incorporated, which has not been covered by any other commercial programs.

References

1. ACI Committee 318. (2014). “Building Code Requirements for Structural Concrete (ACI 318-14) and Commentary (ACI 318R-14).” American Concrete Institute. Farmington Hills, MI.
2. Burns, N. H., Charney, F. A., & Vines, W. R. (1978). “Tests of one-way post-tensioned slabs with unbonded tendons.” *PCI Journal*, 23(5), 66–83.
3. Euler, L. (1783). “De serie Lambertina Plurimisque eius insignibus proprietatibus.” *Acta Academiae Scientiarum Imperialis Petropolitanae*, 2, 29–51.
4. Foutch, D. A., Gamble, W. L., & Sunidja, H. (1990). “Tests of post-tensioned concrete slab-edge column connections.” *ACI Structural Journal*, 87(2), 167–179.
5. Gauss, C. F. (1809). “Theoria motus corporum coelestium sectionibus conicis solem ambientium.” *Werke*, 7, 1–280.
6. Hognestad, E. (1951). “A Study of Combined Bending and Axial Load in Reinforced Concrete Members.” *Bulletin Series No. 399*, 128.
7. KCI. (2012). “2012 Concrete Design Code of KOREA.” Seoul.
8. Kent, D. C., & Park, R. (1971). “Flexural members with confined concrete.” *Journal of the Structural Division*, 97(7), 1969–1990.
9. Lambert, J. (1758). “Observationes variae in mathesin puram.” *Acta Helvetica, Physico-Mathematico-Anatomico-Botanico-Medica*, 3, 128–168.
10. Lee, D. (2010). “Unified Theory on Flexural Behavior of Post-Tensioned Members with Unbonded Tendons.” the University of Seoul.
11. Lim, J.-H., Moon, J.-H., & Lee, L.-H. (1999). “Experimental Examination of Influential Variables on Unbonded Tendon Stresses.” *Journal of the Korea Concrete Institute*, 11(1), 209–219.
12. Mander, J. B., Priestley, M. J. N., & Park, R. (1988). “Theoretical Stress-Strain Model for Confined Concrete.” *Journal of Structural Engineering*, 114(8), 1804–1826.
13. Marrey, B., & Grote, J. (2003). “The story of prestressed concrete from 1930 to 1945: A step towards the European Union.” *Proceedings of the*

First International Congress on Construction History, 1369-1376.

14. Mattock, A. (1979). "Flexural strength of prestressed concrete sections by programmable calculator." *PCI Journal*, 24(1), 32–54.
15. Menegotto, M., & Pinto, P. E. (1973). "Method of Analysis for Cyclically Loaded R. C. Plane Frames Including Changes in Geometry and Non-Elastic Behavior of Elements under Combined Normal Force and Bending." *Proceedings of IABSE Symposium on Resistance and Ultimate Deformability of Structures Acted on by Well Defined Loads*, 15–22.
16. Naaman, A. E. (1977). "Ultimate analysis of prestressed and partially prestressed sections by strain compatibility." *PCI Journal*, 22(1), 32–51.
17. Naaman, A. E., Burns, N., French, C., Gamble, W. L., & Mattock, A. H. (2002). "Stresses in unbonded prestressing tendons at ultimate: Recommendation." *ACI Structural Journal*, 99(4), 518–529.
18. Park, R., Priestley, M. J. N., & Gill, W. D. (1982). "Ductility of Square-Confined Concrete Columns." *Journal of the Structural Division*, 108(4), 929–950.
19. PCI Industry Handbook Committee. (2010). "PCI Design Handbook: Precast and Prestressed Concrete." Precast Concrete Institute.
20. Popovics, S. (1973). "A numerical approach to the complete stress-strain curve of concrete." *Cement and Concrete Research*, 3(5), 583–599.
21. Ramberg, W., & Osgood, W. R. (1943). "Description of stress-strain curves by three parameters." *National Advisory Committee For Aeronautics*, Technical Note No. 902.
22. Saatcioglu, M., & Razvi, S. R. (1992). "Strength and ductility of confined concrete." *Journal of Structural Engineering, ASCE*, 118(6), 1590–1607.
23. Tao, X. K., & Du, G. C. (1985). "Ultimate stress of unbonded tendons in partially prestressed concrete beams." *Journal Prestressed Concrete Institute*, 30(6), 72–91.
24. Wagner, B., Petrussha, R., & Wenzel, M. (2017). "C# programming guide." Retrieved from <https://docs.microsoft.com/en-us/dotnet/csharp/programming-guide/>
25. Wallace, J. W. (1992). "BIAX: revision 1, a computer program for the analysis of reinforced concrete sections." Clarkson University, Department of Civil Engineering.
26. Whitney, C. S. (1937). "Design of Reinforced Concrete Members under Flexure or Combined Flexure and Direct Compression." *ACI Journal Proceedings*, 33(3), 483-498.

27. Yang, K. H., Mun, J. H., Cho, M. S., & Kang, T. H.-K. (2014). "Stress-strain model for various unconfined concretes in compression." *ACI Structural Journal*, *111*(4), 819–826.
28. Zhou, W., & Zheng, W. (2014). "Unbonded Tendon Stresses in Continuous Post-Tensioned Beams." *ACI Structural Journal*, *111*(3).

Appendix A: Program Screenshots and Detailed Description

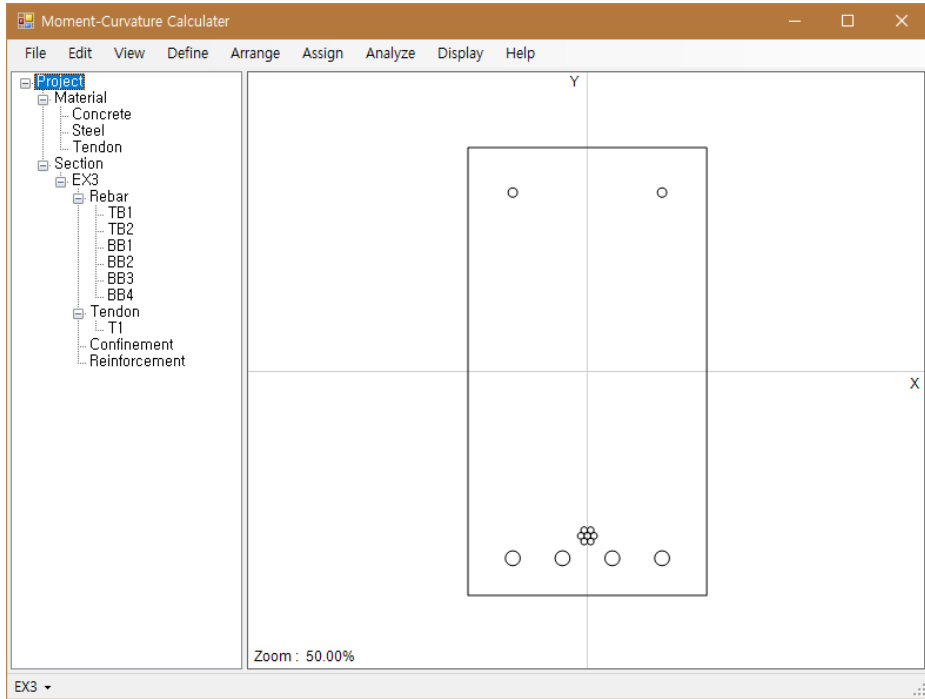
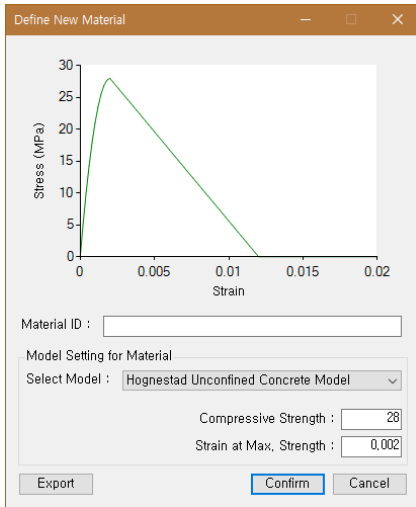


Figure A-1 Main window

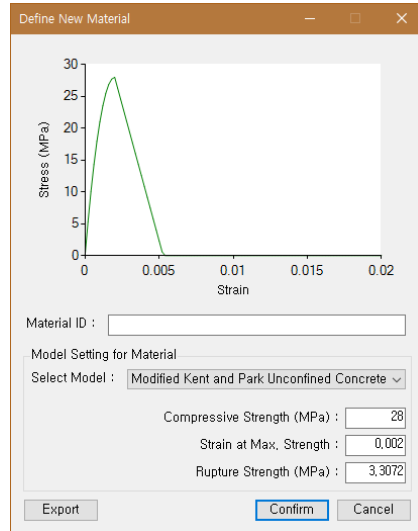
Table A-1 Menu description

Menu	Sub-Menu	Description
File	New	Close the current project and make a new project.
	Open	Open the project file (*.mcc) and load the information.
	Save	Save the current project. If the project is not saved once yet, then “Save as...” menu will be executed instead of this.
	Save as...	Save the current project with a specific filename.
	Close	Close the project and exit the program.
Edit	Delete	Delete the selected item of tree view on the left side.
	Replicate...	Replicate the selected component of tree view on the left side. User can replicate rebars with a

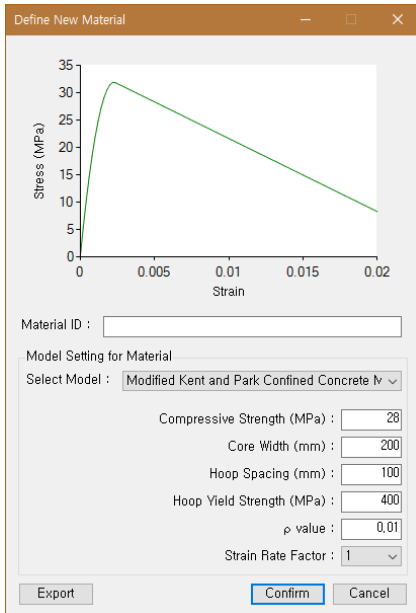
		specific offset in any direction.
View	Refresh	Refresh the cross-sectional view. Basically, the cross-sectional view is automatically refreshed whenever users do something.
	Zoom In	Zoom in the cross-sectional view. The minimum magnification is 10%
	Zoom Out	Zoom out the cross-sectional view. The maximum magnification is 500%.
	Fit to Window	Make the cross-sectional view fit to the window so that user can see the entire cross-section.
	Show ID	Show the IDs of structural components on the cross-sectional view
	Show Material ID	Show the material IDs on the cross-sectional view
Define	Material...	Define a new material model
	Section...	Define a new section
Arrange	Rebar...	Add a new rebar component to the current section.
	Tendon...	Add a new tendon component to the current section.
	Structural Steel...	Add a new structural steel (e.g. I steel beam) to the current section.
Assign	Corner Rebars...	Set the confined area through selecting the four corners of transverse reinforcement.
Analyze	Options...	Giving sectional analysis options. (Refer to Table 4-2)
	Run Analysis	Start running the whole analysis. Progress bar will be displayed.
Display	Moment-Curvature	Display the chart of moment-curvature relations with colors.
	P-M Interaction	Display the chart of P-M interactions.
Help	Manual	Display the manual.
	Version	Display the current version of program.



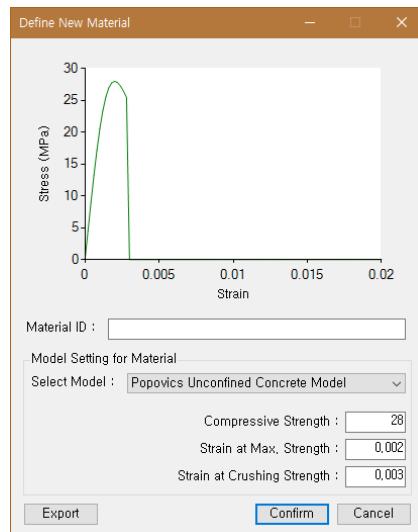
(a) Hognestad unconfined concrete model



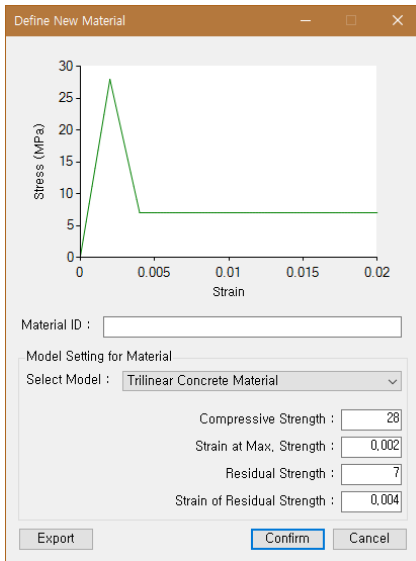
(b) Modified Kent and Park unconfined concrete model



(c) Modified Kent and Park confined concrete model



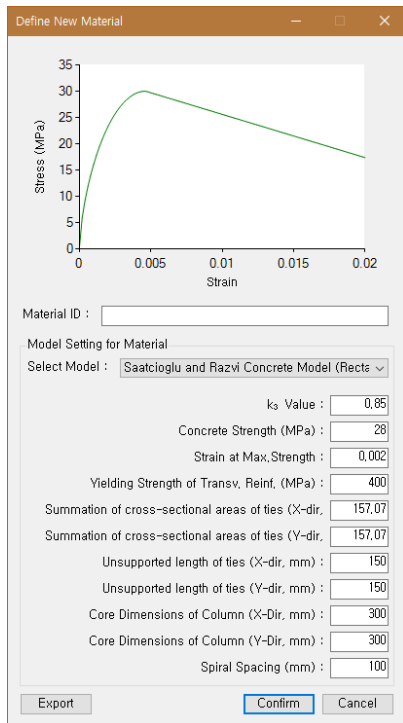
(d) Popovics unconfined concrete model



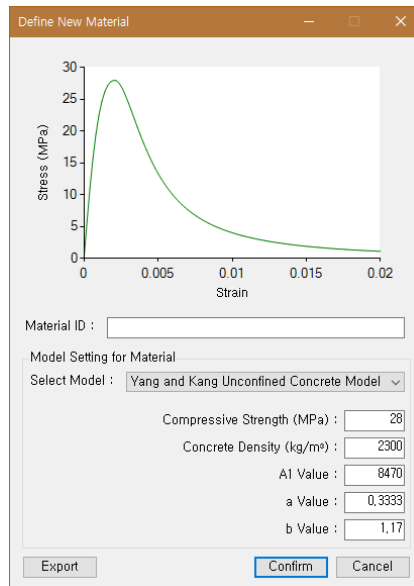
(e) Trilinear concrete model



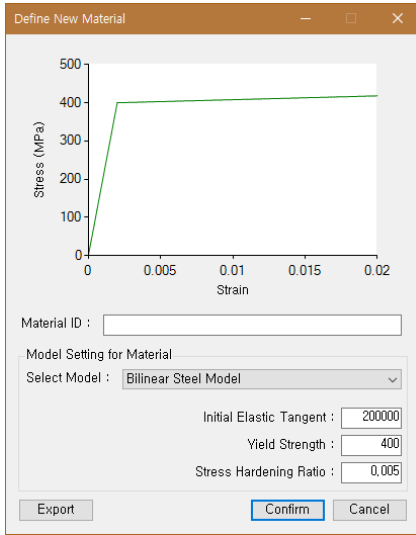
(f) Saatcioglu and Razvi confined concrete model (Circular)



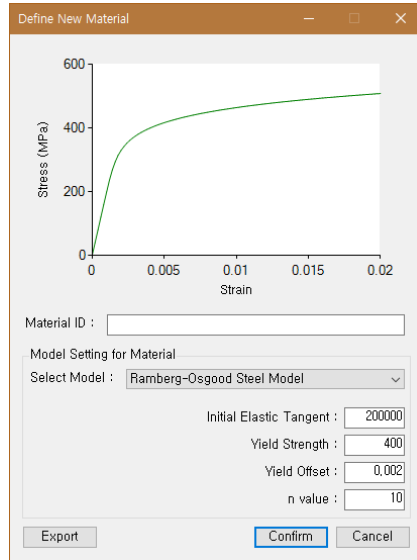
(g) Saatcioglu and Razvi confined concrete model (Rectangular)



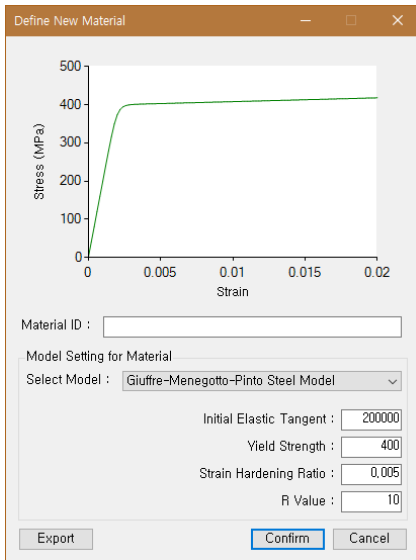
(h) Yang et al. unconfined concrete model



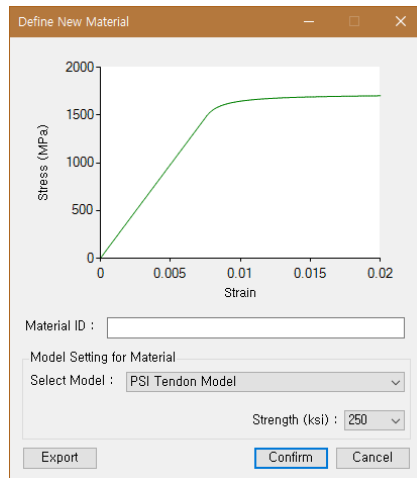
(i) Bilinear steel model



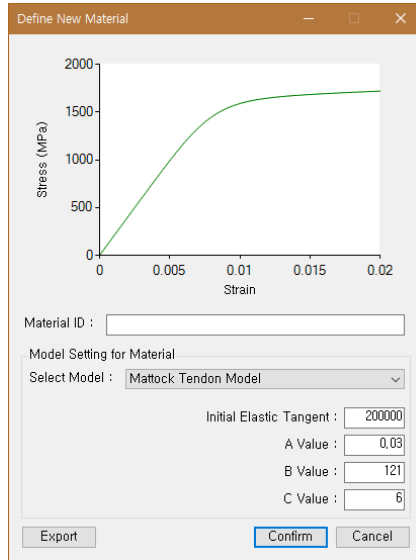
(j) Ramber-Osgood steel model



(k) Menegotto-Pinto steel model

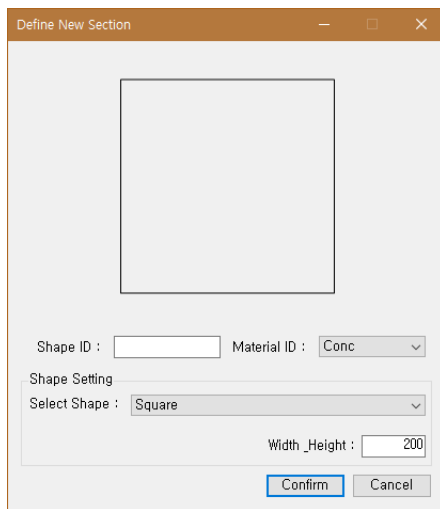


(l) PCI tendon model

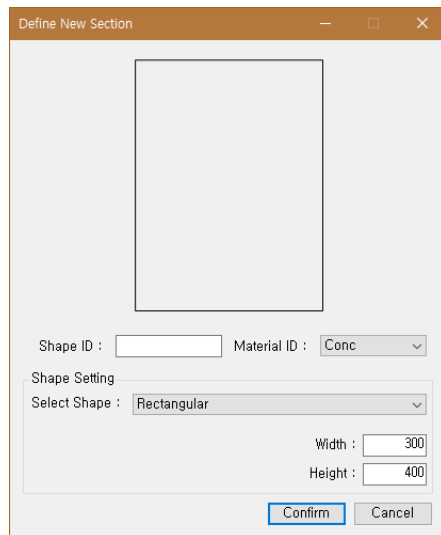


(m) Mattock tendon model

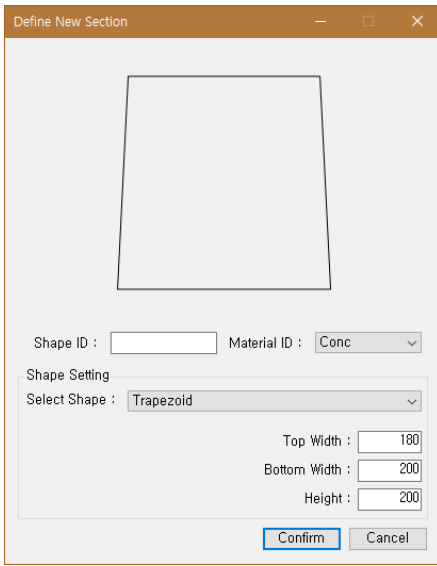
Figure A-2 Supported material models and user interface



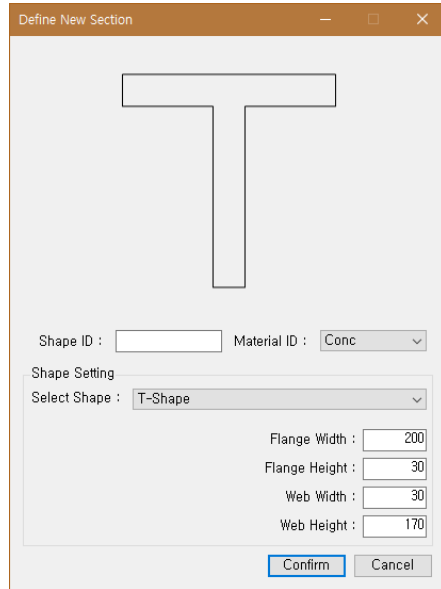
(a) Square cross-section



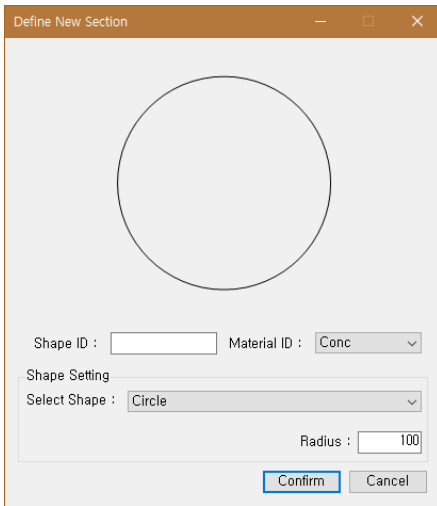
(b) Rectangular cross-section



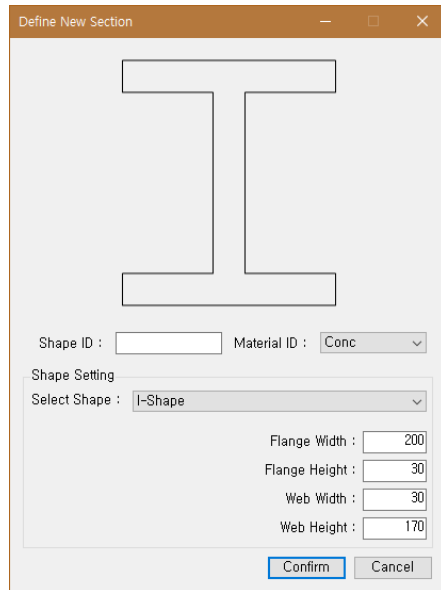
(c) Trapezoid cross-section



(d) T shaped cross-section



(e) Circular cross-section



(f) I shaped cross-section

Figure A-3 Supported sectional shape and user interface when defining new section

Arrange Rebar

Rebar ID : Material ID :

Rebar Property

Location X (mm) : Area (mm²) :

Location Y (mm) : Diameter (mm) :

Figure A-4 User interface for arranging rebars

Arrange Tendon

Tendon ID : Material ID :

Tendon Setting

Location X (mm) : Area (mm²) :

Location Y (mm) : Diameter (mm) :

Tendon Initial Stress (MPa) :

Post-Tension Setting

Post-Tensioning :

Δf_{ps} (MPa) :

Figure A-5 User interface for arranging tendons

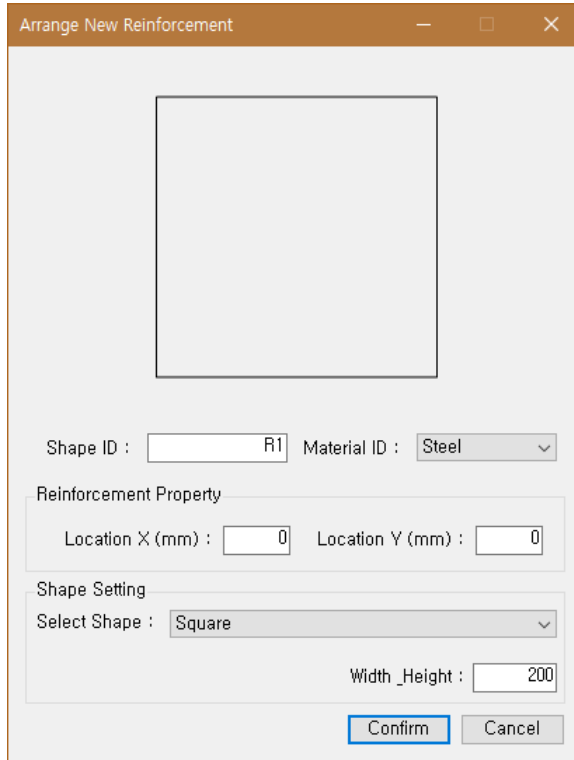


Figure A-6 User interface for arranging structural steel

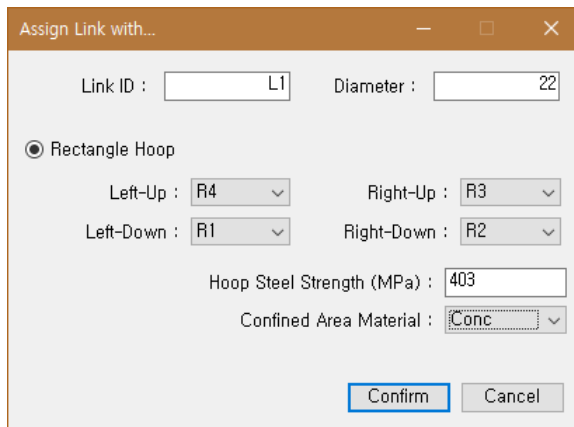


Figure A-7 User interface for setting four corners of confined area

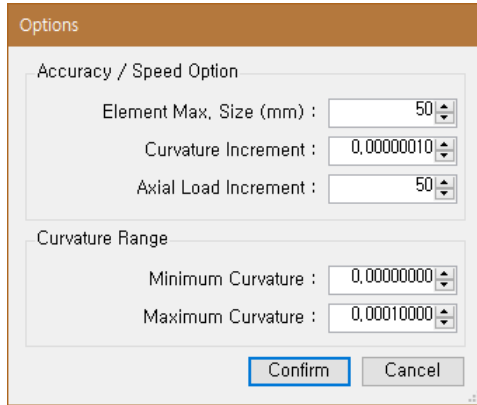


Figure A-8 User interface for setting analysis options

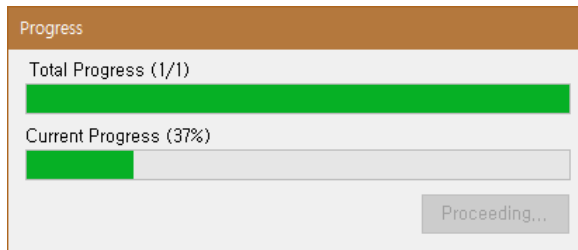


Figure A-9 Window for displaying analysis progresses

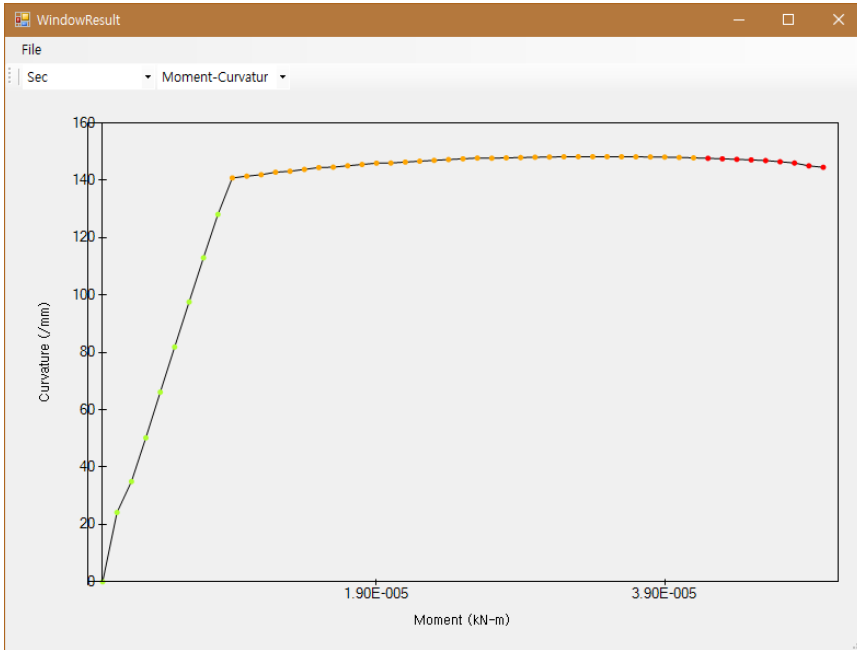


Figure A-10 Result window for moment-curvature relation

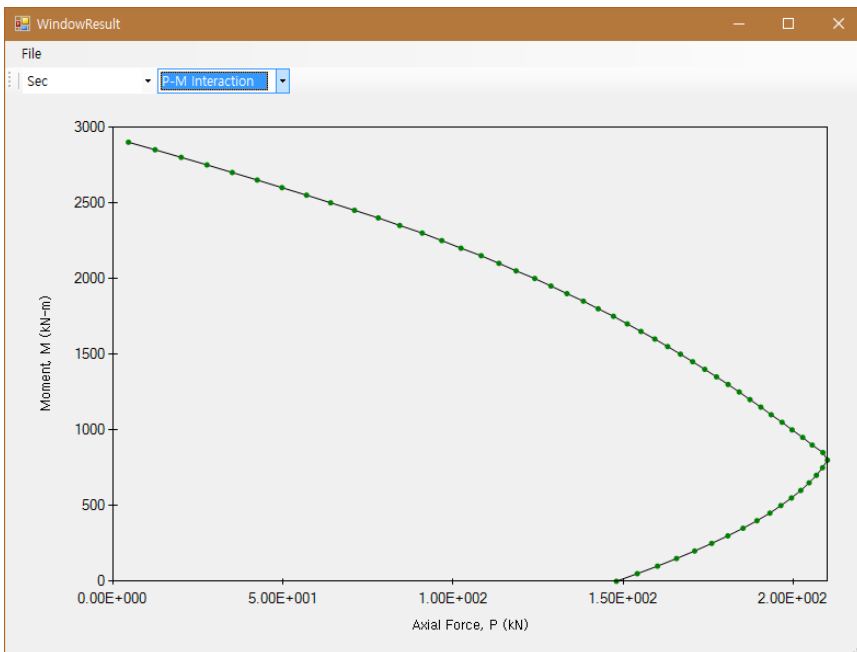


Figure A-11 Result window for P-M interaction

Appendix B: Simple User Manual for Program

B.1 Define Material

1. Select **Define > Material...** from the top menu bar of main window.
2. Set **Material ID** for recognizing the defined model. **Material ID** must be unique.
3. Select material model at **Select Model** combo box. The parameter input UIs will be changed as the model is selected.
4. Set all parameters for the selected model. Some parameters are set by textbox, while the other parameters are set by combo box. The parameters with combo box cannot be set freely and they are limited to several specific values by the model itself. (e.g. **Strain Rate Factor** of the modified Kent and Park confined concrete model is set through selecting among the specific values, 1 and 1.25, with combo box . (**Figure A-2** (e))
5. Press **Confirm** button. For obtaining the stress-strain information as file, then press **Export** button and save the data.

B.2 Define Section

1. Select **Define > Section...** from the top menu bar of main window. If any material model is not registered, the error message box will be shown.
2. Set **Section ID** for recognizing the defined model. **Section ID** must be unique.
3. Select **Material ID** for the section. In this step, only concrete material models among the models added at **B.1** will appear.
4. Select the cross-sectional shape at **Select Shape** combo box. The

parameter input UIs will be changed as the shape is selected.

5. Set all parameters for the selected shape.
6. Press **Confirm** button.

B.3 Add Reinforcements

Go to **Arrange** menu and select among three reinforcement items: rebar, tendon and structural steel.

B.3.1 Rebar

1. Set **Rebar ID** for recognizing the defined rebar item. **Rebar ID** must be unique.
2. Select **Material ID** for the defined rebar item. In this step, only steel material models among the models added at **B.1** will appear.
3. Set X and Y coordinates. The position standard is already shown in the cross-sectional view on main window.
4. Set area or diameter parameter. Once the one is set, then the other will be set automatically.
5. Press **Confirm** button.

B.3.2 Tendon

1. Set **Tendon ID** for recognizing the defined tendon item. **Tendon ID** must be unique
2. Select **Material ID** for the defined rebar item. In this step, only tendon material models among the models added at **B.1** will appear.
3. Set X and Y coordinates.

4. Set area or diameter parameter.
5. Set **Tendon Effective Stress**. This value should be given by user.
6. Set **Setting for Unbonded Post-Tensioning**. Check if the defined tendon item is unbonded. Then Δf_{ps} parameter input textbox will be enabled. User should calculate this value according to f_{ps} prediction models. (e.g. Naaman et al. (2002))
7. Press **Confirm** button.

B.3.3 Structural Steel

1. Set **Structural Steel ID** for recognizing the defined structural steel item. **Structural Steel ID** must be unique.
2. Select **Material ID** for the defined structural steel item. In this step, only steel material models among the models added at **B.1** will appear.
3. Set X and Y coordinates.
4. Select the cross-sectional shape at **Select Shape** combo box. The parameter input UIs will be changed as the shape is selected.
5. Set all parameters for the selected shape.
6. Press **Confirm** button.

B.4 Assign Confined Area

1. Select **Assign > Corener Rebars...** from the top menu bar of main window.
2. Set **Link ID** for recognizing the confinement hoop item. **Link ID**

must be unique.

3. Select the **Rebar IDs** on combo boxes for four corners of the confinement hoop.
4. Press **Confirm** button.

B.5 Check Analysis Options

Check the analysis options for controlling the accuracy, the speed and the range of curvature of the analysis. The detailed information about the analysis options is described in **Table 4-2**.

B.6 Run Analysis and Obtain the Result

1. Select **Analyze > Run Analysis** from the top menu bar of main window.
2. The progress will be displayed. There is a disabled button saying “Proceeding...” on the right-bottom side. The analysis process is finished, then the button will be enabled with the text “Finish”. Press the Finish Button
3. Select **Display > Moment-Curvature** or **Display > P-M Interaction** from the top menu bar of main window. The display show a line graph on the chart. You can change the graph by selecting the items of combo boxes on the toolbar.
4. Select **File > Export Current Data (*.csv)** for exporting the graph data as a file. The exported file can be opened using other spreadsheet programs like Microsoft Excel.

국 문 초 록

철근콘크리트와 프리스트레스트 콘크리트 단면해석 플랫폼 구축 연구

주요 구조부재로서 프리스트레스트 콘크리트의 중요성은 점점 더 부각되고 있다. 하지만 프리스트레스트 콘크리트 부재에 대한 단면해석 연구는 아직 실무적으로 미비한 실정이다. 3 차원 유한요소법을 이용한 해석은 거동을 이해하는데 좋은 방법일 수 있지만, 많은 컴퓨터 자원과 시간이 소요되므로 다소 실무적이지 않다. 따라서, 포스트텐션 무량판 구조물 등과 같은 프리스트레스트 콘크리트 건물 전체에 대하여 비선형 해석을 효과적으로 수행하기 위해서는 변위기반 설계법을 위한 소성 힌지 모델링이 요구된다. 본 연구에서는 비부착 프리스트레스트 콘크리트 부재를 포함하여 모든 콘크리트 부재에 대한 모멘트-곡률 곡선 및 P-M 관계도 산출 프로그램을 개발하였다. 이를 위해 기존의 비부착 프리스트레스트 콘크리트 실험결과들을 취합 정리한 후, 강연선 응력 증가와 부재에 작용하는 힘 또는 모멘트간의 관계식을 도출하여 이 프로그램에 적용하였다. 프로그램은 C#를 이용하여 개발되었으며, 비부착 프리스트레스트 콘크리트 부재를 포함한 다양한 조건의 단면에

대하여 모멘트-곡률 곡선 및 P-M 관계도를 편리하게 산출해 낼 수 있도록 구성되었다. 프로그램으로부터 산출된 결과 중 일반 철근 콘크리트와 부착 프리스트레스트 콘크리트 부재에 대해서 기존의 검증된 단면해석 프로그램 및 타 프로젝트와의 비교를 통해 정확도를 검증하였다. 반면 비부착 프리스트레스트 콘크리트의 경우 기존의 단면해석 프로그램이나 도출된 곡선 또는 관계도가 없기 때문에 다양한 조건의 강연선 응력 증가 모델을 이용한 변수 연구를 진행하였다. 이를 통해 강연선 응력의 선형 및 지수적 응력 증가 모델이 모멘트-곡률 곡선 산출에 있어 적합한 것으로 나타났다.

핵심용어: 단면해석, 철근 콘크리트, 부착 프리스트레스트 콘크리트, 비부착 프리스트레스트 콘크리트, 모멘트-곡률 곡선, P-M 관계도
학번: 2015-22847